Langmuir
Article
pubs.acs.org/Langmuir

How Does Bone Sialoprotein Promote the Nucleation of Hydroxyapatite? A Molecular Dynamics Study Using Model Peptides of Different Conformations

Yang Yang,[†] Qiang Cui,[‡] and Nita Sahai*[,†,§,⊥]

[†]*Department of Geoscience, University of Wisconsin, Madison, 1215 West Dayton Street, Madison, Wisconsin 53706,* [‡]*Department of Chemistry and Theoretical Chemistry Institute, University of Wisconsin, Madison, 1101 University Avenue, Madison, Wisconsin 53706,* [§]*Materials Science Program, University of Wisconsin, Madison, 1509 University Avenue, Madison, Wisconsin 53706, and* [⊥]*Environmental Chemistry and Technology Program, University of Wisconsin, Madison, 680 North Park Street, Madison, Wisconsin 53706*

Received January 14, 2010. Revised Manuscript Received April 26, 2010

Bone sialoprotein (BSP) is a highly phosphorylated, acidic, noncollagenous protein in bone matrix. Although BSP has been proposed to be a nucleator of hydroxyapatite ($Ca_5(PO_4)_3OH$), the major mineral component of bone, no detailed mechanism for the nucleation process has been elucidated at the atomic level to date. In the present work, using a peptide model, we apply molecular dynamics (MD) simulations to study the conformational effect of a proposed nucleating motif of BSP (a phosphorylated, acidic, 10 amino-acid residue sequence) on controlling the distributions of Ca^{2+} and inorganic phosphate (Pi) ions in solution, and specifically, we explore whether a nucleating template for orientated hydroxyapatite could be formed in different peptide conformations. Both the α-helical conformation and the random coil structure have been studied, and inorganic solutions without the peptide are simulated as reference. Ca^{2+} distributions around the peptide surface and interactions between Ca^{2+} and Pi in the presence of the peptide are examined in detail. From the MD simulations, although in some cases for the α-helical conformation, we observe that a Ca^{2+} equilateral triangle forms around the surface of peptide, which matches the distribution of Ca^{2+} ions on the (001) face of the hydroxyapatite crystal, we do not consistently find a stable nucleating template formation in general for either the helical conformation or the random coil structure. Therefore, independent of conformations, the BSP nucleating motif is more likely to help nucleate an amorphous calcium phosphate cluster, which ultimately converts to crystalline hydroxyapatite.

1. Introduction

Bone is a complex hierarchical material that provides a structural support for vertebrates.[1,2] The inorganic phase of the bone is a nonstoichiometric hydroxyapatite-like ($Ca_5(PO_4)_3OH$) nanocrystalline mineral in specific spatial relationship to a collagen matrix. Several noncollagenous proteins are also associated with the mineral phase. Thus, the growth of bone is controlled by naturally evolved proteins.[2−8] Malfunction of these proteins or calcium or vitamin deficiencies may lead to severe skeleton-related diseases,[9] such as rickets, osteogenesis imperfect and osteoporosis. Therefore, understanding the mechanism of bone formation and growth *in vivo* is of fundamental biomedical importance. Because protein-ion and protein-mineral surface interactions are expected to play essential roles during the process, the study of protein-controlled hydroxyapatite mineralization is also interesting from a physical chemistry point of view.[10]

Bone sialoprotein (BSP) is one of the major noncollagenous proteins in bones.[11] Mammalian BSP has ∼327 amino acids, with a molecular weight of 33−34 kDa.[4,11,12] Extensive post-translational modifications, which involve Ser/Thr/Tyr phosphorylation, Tyr sulfation and N/O-linked glycosylation, increase the apparent molecular weight to ∼75 kDa for a mature BSP.[13−20] A large number of Glu residues (around 22% of the total amino acids) plus phosphate and sulfate groups make BSP highly acidic.[21] In addition, it is found that BSP transcripts are expressed at a high level in areas of *de novo* bone formation[22−27] during the

*To whom correspondence should be addressed. E-mail: sahai@geology.wisc.edu. Telephone: 608-262-4972. Fax: 608-262-0693.

(1) Glimcher, M. J. *Rev. Mineral. Geochem.* **2006**; *64*, 223.
(2) Steele, D. G.; Bramblett, C. A. *The Anatomy and Biology of the Human Skeleton*; Texas A&M University, College Station Press: College Station, TX, 1988.
(3) Mann, S. *Biomineralization Principles and Concepts in Bioinorganic Materials Chemistry*; Oxford Univeristy Press: Oxford, U.K., 2001.
(4) George, A.; Veis, A. *Chem. Rev.* **2008**, *108*, 4670.
(5) Boskey, A. L. *Connect. Tissue. Res.* **2003**, *44*, 5.
(6) Boskey, A. L. *Phosphorus, Sulfur Silicon Relat. Elem.* **1999**, *146*, 189.
(7) Boskey, A. L. *Ann. N.Y. Acad. Sci.* **1995**, *760*, 249.
(8) Alford, A. I.; Hankenson, K. D. *Bone* **2006**, *38*, 749.
(9) Boskey, A. L. In *Bone Mechanics Handbook*; Cowin, S. C., Ed.; CRC Press: Boca Raton, FL, 2000; p 5.1−5.31.
(10) Gray, J. J. *Curr. Opin. Struc. Biol.* **2004**, *14*, 110.
(11) Ganss, B.; Kim, R. H.; Sodek, J. *Crit. Rev. Oral. Biol. M.* **1999**, *10*, 79.
(12) Tye, C. E.; Rattray, K. R.; Warner, K. J.; Gordon, J. A. R.; Sodek, J.; Hunter, G. K.; Goldberg, H. A. *J. Biol. Chem.* **2003**, *278*, 7949.
(13) Fisher, L. W.; Mcbride, O. W.; Termine, J. D.; Young, M. F. *J. Biol. Chem.* **1990**, *265*, 2347.
(14) Zhu, X. L.; Ganss, B.; Goldberg, H. A.; Sodek, J. *Biochem. Cell Biol.* **2001**, *79*, 737.
(15) Sorensen, E. S.; Hojrup, P.; Petersen, T. E. *Protein Sci.* **1995**, *4*, 2040.
(16) Franzen, A.; Heinegard, D. *Biochem. J.* **1985**, *232*, 715.
(17) Salih, E.; Zhou, H. Y.; Glimcher, M. J. *J. Biol. Chem.* **1996**, *271*, 16897.
(18) Zaia, J.; Boynton, R.; Heinegard, D.; Barry, F. *Biochemistry* **2001**, *40*, 12983.
(19) Salih, E. *Connect. Tissue Res.* **2003**, *44*, 223.
(20) Ecarotcharrier, B.; Bouchard, F.; Delloye, C. *J. Biol. Chem.* **1989**, *264*, 20049.
(21) Gorski, J. P. *Calcif. Tissue Int.* **1992**, *50*, 391.
(22) Bianco, P.; Fisher, L. W.; Young, M. F.; Termine, J. D.; Robey, P. G. *Calcif. Tissue Int.* **1991**, *49*, 421.
(23) Bianco, P.; Riminucci, M.; Silvestrini, G.; Bonucci, E.; Termine, J. D.; Fisher, L. W.; Robey, P. G. *J. Histochem. Cytochem.* **1993**, *41*, 193.
(24) Chen, J.; Mckee, M. D.; Nanci, A.; Sodek, J. *Histochem. J.* **1994**, *26*, 67.
(25) Chen, J. K.; Singh, K.; Mukherjee, B. B.; Sodek, J. *Matrix* **1993**, *13*, 113.
(26) Hultenby, K.; Reinholt, F. P.; Norgard, M.; Oldberg, A.; Wendel, M.; Heinegard, D. *Eur. J. Cell Biol.* **1994**, *63*, 230.

early phase of bone deposition.[28,29] On the basis of the anionic nature and its spatial and temporal expression levels associated with bone mineralization, BSP has been suggested as a potential nucleator of hydroxyapatite, the dominant component of bone.[7,27,30−33] *In vitro*, this proposal has been verified by Hunter et al., who showed that BSP is capable of promoting hydroxyapatite nucleation in a steady-state agarose gel.[34] Blood and the extracellular medium from which bone grows is supersaturated with respect to hydroxyapatite, but the presence of inhibitors such as fetuin prevents nucleation except at specific bone-forming sites. So almost any factor such as a ligand, protein, or inorganic surface capable of lowering the nucleation barrier may induce *in vitro* nucleation. It is therefore, a question of which factor is more efficient as a promoter, rather than whether it is a promoter.

Thus, despite extensive research to study the effect of BSP on the nucleation of hydroxyapatite,[12,21,31,32,34−41] the precise role of BSP is still far from being elucidated.[4,11] Lack of experimental structural information on BSP at the atomic level (both in solution and bound with hydroxyapatite surface) is one of the major obstacles. Unlike many other proteins, where stable three-dimensional structures exist to provide structural support for catalyzing chemical reactions, BSP is predicted to have an open, extended, and flexible structure with the potential to form regions of α-helix and β-sheet in solution, based on the secondary structure and hydrophilicity analyses and one-dimensional proton NMR study.[42,43] By using electron microscopy, Franzén et al. observed that BSP appeared as an extended rod, having a core with an average length of 40 nm.[16] By using circular dichroism and small-angle X-ray scattering, Tye et al. studied the structure of rat BSP in solution, and observed an unfolded protein with no evident secondary structure.[12]

In BSP, two highly conserved Glu-rich domains were demonstrated to have nucleating activity.[36,37] In human BSP, contiguous Glu sequences are found from residue 78 to 85 and from residue 158 to 185.[13] Earlier site-directed mutagenesis study by Tye et al. indicated that a sequence of at least eight contiguous Glu residues is required for BSP to nucleate hydroxyapatite.[12] Because of the anionic nature of the polyglutamic acid, it is not difficult to hypothesize that an appropriate spatial arrangement of γ-carboxylate groups may favor specific Ca^{2+} distribution and therefore promote nucleation; however, whether such a hypothesis is valid, and if so, what the precise stereochemical arrangement of nucleating groups is remain elusive.[5,11]

Theoretical modeling, in principle, affords us a means to assemble the available experimental information and provide insights into the nucleating mechanisms and other biomineralization processes with atomic details.[10,44−51] Using a fragment of the calcium ortho-phosphoserine crystal structure to represent a sequence consisting of one phosphorylated serine and two glutamates as the model for the nucleating motif of BSP, one of us carried out a structural study of Ca^{2+} and inorganic phosphate complexes based on *ab initio* quantum calculations of the potential energy surface.[41] In that work, an interesting matching pattern was noted between the arrangement of phosphate and carboxylate groups and the phosphate ion distributions on the (001) face of the hydroxyapatite. It was found that carboxylate and phosphate ester groups are arranged at 60° from each other with the Ca^{2+} ion at the center of the equilateral triangle, identical to the phosphate and Ca^{2+} ion distributions on the (001) face of the hydroxyapatite. It was, therefore, proposed that the nucleating motif of BSP consists of a phosphorylated serine and two glutamates that are arranged in such a way that their anionic residues form an equilateral triangle for Ca^{2+} to bind. However, due to the lack of thermal fluctuations, the role of the peptide could not be confirmed.

In the present work, we use molecular dynamic (MD) simulations to explore the possible roles of the BSP in the nucleation of hydroxyapatite. Of the two Glu-rich domains in human BSP, a peptide sequence in the domain closer to the N-terminus is selected for study (see Methods). Water molecules are explicitly included. The entire system is described with the CHARMM force field.[52−54] We try to verify whether nucleation templates may form with peptide in different conformations which facilitate the direct nucleation of crystalline hydroxyapatite. Thus, the conformational effect of the peptide on the distributions of Ca^{2+} ions and inorganic phosphate (Pi) is the focus of the current study. Long period simulations (some are up to ∼35 ns) are performed to address the dynamic features of the solution system.

Though the polyglutamic acids sequences have been suggested to be critical for the nucleation of hydroxyapatite, no clear evidence concerning their structure is available.[4,11] In order to explore the dependence of the ion distribution on the peptide conformation, we have studied both structured and unstructured conformations. For the former, we assume that

(27) Chen, J. K.; Shapiro, H. S.; Wrana, J. L.; Reimers, S.; Heersche, J. N. M.; Sodek, J. *Matrix* **1991**, *11*, 133.
(28) Kasugai, S.; Nagata, T.; Sodek, J. *J. Cell. Physiol.* **1992**, *152*, 467.
(29) Riminucci, M.; Bradbeer, J. N.; Corsi, A.; Gentili, C.; Descalzi, F.; Cancedda, R.; Bianco, P. *J. Bone Miner. Res.* **1998**, *13*, 1852.
(30) Stubbs, J. T.; Mintz, K. P.; Eanes, E. D.; Torchia, D. A.; Fisher, L. W. *J. Bone Miner. Res.* **1997**, *12*, 1210.
(31) Hunter, G. K.; Goldberg, H. A. *Biochem. J.* **1994**, *302*, 175.
(32) Harris, N. L.; Rattray, K. R.; Tye, C. E.; Underhill, T. M.; Somerman, M. J.; D'Errico, J. A.; Chambers, A. F.; Hunter, G. K.; Goldberg, H. A. *Bone* **2000**, *27*, 795.
(33) Hunter, G. K. *Curr. Opin. Solid State Mater. Sci.* **1996**, *1*, 430.
(34) Hunter, G. K.; Goldberg, H. A. *Proc. Natl. Acad. Sci. U.S.A.* **1993**, *90*, 8562.
(35) Harris, N. L.; Hunter, G. K.; Somerman, M. J.; DErrico, J. A.; Goldberg, H. A. *J. Dent. Res.* **1997**, *76*, 2180.
(36) Goldberg, H. A.; Hunter, G. K. *J. Dent. Res.* **1994**, *73*, 282.
(37) Goldberg, H. A.; Warner, K. J.; Stillman, M. J.; Hunter, G. K. *Connect. Tissue Res.* **1996**, *35*, 385.
(38) Hunter, G. K.; Hauschka, P. V.; Poole, A. R.; Rosenberg, L. C.; Goldberg, H. A. *Biochem. J.* **1996**, *317*, 59.
(39) Tye, C. E.; Hunter, G. K.; Goldberg, H. A. *J. Dent. Res.* **2002**, *81*, A477.
(40) Matsumoto, T.; Okazaki, M.; Inoue, M.; Sasaki, J. I.; Hamada, Y.; Takahashi, J. *Dent. Mater. J.* **2006**, *25*, 360.
(41) Sahai, N. *Am. J. Sci.* **2005**, *305*, 661.
(42) Shapiro, H. S.; Chen, J. K.; Wrana, J. L.; Zhang, Q.; Blum, M.; Sodek, J. *Matrix* **1993**, *13*, 431.
(43) Fisher, L. W.; Torchia, D. A.; Fohr, B.; Young, M. F.; Fedarko, N. S. *Biochem. Biophys. Res. Commun.* **2001**, *280*, 460.
(44) Harding, J. H.; Duffy, D. M. *J. Mater. Chem.* **2006**, *16*, 1105.
(45) Harding, J. H.; Duffy, D. M.; Sushko, M. L.; Rodger, P. M.; Quigley, D.; Elliott, J. A. *Chem. Rev.* **2008**, *108*, 4823.
(46) Latour, R. A. *Biointerphases* **2008**, *3*, Fc2.
(47) Di Tommaso, D.; de Leeuw, N. H. *J. Phys. Chem. B* **2008**, *112*, 6965.
(48) Di Tommaso, D.; de Leeuw, N. H. *Geochim. Cosmochim. Acta* **2009**, *73*, 5394.
(49) Greathouse, J. A.; Cygan, R. T.; Bradshaw, R. W.; Majzoub, E. H.; Simmons, B. A. *J. Phys. Chem. C* **2007**, *111*, 16787.
(50) Cygan, R. T.; Liang, J. J.; Kalinichev, A. G. *J. Phys. Chem. B* **2004**, *108*, 1255.
(51) Latour, R. A. *Curr. Opin. Solid State Mater. Sci.* **1999**, *4*, 413.
(52) MacKerell, A. D.; Bashford, D.; Bellott, M.; Dunbrack, R. L.; Evanseck, J. D.; Field, M. J.; Fischer, S.; Gao, J.; Guo, H.; Ha, S.; Joseph-McCarthy, D.; Kuchnir, L.; Kuczera, K.; Lau, F. T. K.; Mattos, C.; Michnick, S.; Ngo, T.; Nguyen, D. T.; Prodhom, B.; Reiher, W. E.; Roux, B.; Schlenkrich, M.; Smith, J. C.; Stote, R.; Straub, J.; Watanabe, M.; Wiorkiewicz-Kuczera, J.; Yin, D.; Karplus, M. *J. Phys. Chem. B* **1998**, *102*, 3586.
(53) Brooks, B. R.; Bruccoleri, R. E.; Olafson, B. D.; States, D. J.; Swaminathan, S.; Karplus, M. *J. Comput. Chem.* **1983**, *4*, 187.
(54) Brooks, B. R.; Brooks, C. L.; Mackerell, A. D.; Nilsson, L.; Petrella, R. J.; Roux, B.; Won, Y.; Archontis, G.; Bartels, C.; Boresch, S.; Caflisch, A.; Caves, L.; Cui, Q.; Dinner, A. R.; Feig, M.; Fischer, S.; Gao, J.; Hodoscek, M.; Im, W.; Kuczera, K.; Lazaridis, T.; Ma, J.; Ovchinnikov, V.; Paci, E.; Pastor, R. W.; Post, C. B.; Pu, J. Z.; Schaefer, M.; Tidor, B.; Venable, R. M.; Woodcock, H. L.; Wu, X.; Yang, W.; York, D. M.; Karplus, M. *J. Comput. Chem.* **2009**, *30*, 1545.

the peptide adopts an α-helical conformation, as proposed by Hunter et al.[31] This assumption is further tested using the Robetta server,[55−58] a knowledge-based protein structure prediction program; the secondary structure of the polyglutamic acid sequence is predicted to be helical with the PSIPRED method.[59] For the unstructured conformation, a random coil structure is prepared.

Two serine amino acids immediately precede the studied polyglutamic acid sequence are highly conserved in mammalian BSPs (e.g., human, pig, cow, rat, mouse, and hamster).[11] These two serine residues are phosphorylated by casein kinase II or protein kinase C during post-translational modifications.[17,19] The role of phosphate groups in biomineralization is under debate.[1,6,31,60−62] Because of the negative charge, phosphate groups may sequester calcium and thereby help nucleate hydroxyapatite. However, Hunter and Goldberg observed that the nucleation activity of BSP is not apparently influenced by enzymatic dephosphorylation.[31] On the other hand, because the body fluid is supersaturated with respect to the hydroxyapatite, any factor that reduces the nucleation barrier is expected to promote hydroxyapatite nucleation including a Glu sequence without phosphorylated serine. Thus, it is actually a question of which factor is more efficient rather than whether either one can promote nucleation or not. In the present work, therefore, we include both phosphorylated serines and polyglutamic acid sequence in the peptide model. The effects of peptide conformations on interactions between the Glu side chains, phosphorylated Ser, and Ca^{2+}/Pi are the subjects of interest. Specifically, Ca^{2+} distributions around the peptide surface and interactions between Ca^{2+} and Pi in the presence of the peptide are examined in detail to identify features that may promote hydroxyapatite nucleation in solution.

When the peptide adopts an α-helical conformation, in some of the simulations, we observe that a Ca^{2+} equilateral triangle forms around the peptide surface; this configuration matches the distribution of Ca^{2+} ions on the (001) face of the hydroxyapatite crystal. It seems to imply one possible role of the α-helical conformation of the BSP nucleating motif is to promote the nucleation of the oriented hydroxyapatite crystal by templating the distribution of Ca^{2+} ions. However, the formation of the Ca^{2+} equilateral triangle template is not general and some of the equilateral triangle templates formed break up along the course of the longer simulations. When the peptide adopts a random coil conformation, the distribution of Ca^{2+} ions from the simulations does not indicate an apparent nucleation template. Therefore, independent of conformation, the BSP nucleating motif is more likely to promote amorphous calcium phosphate cluster, which ultimately converts to crystalline hydroxyapatite, though the possibility of nucleation of the crystalline hydroxyapatite exists for the helical conformation due to the template promotion. In the following, computational methods are given in section 2. Results and discussions are shown in sections 3 and 4 respectively. Finally, we draw a few conclusions in section 5.

2. Methods

2.1. System Setup. *2.1.1. Peptide Structure Setup.* In the present work, one of the two highly conserved glutamic-acid rich sequences in BSP (residues 76−85 of human BSP) is studied using peptide models. The primary sequence of the peptide is SpSpEEEEEEEE, where Sp refers to a phosphorylated serine. Both −1 and −2 protonation states of phosphate groups are considered for neutral pH; all Glu residues are taken to be deprotonated despite their spatial proximity, which is reasonable considering the high ionic strength for conditions of interest. Thus, the model peptide bears either −10 or −12 net charges, depending on the phosphate protonation state. The −12 charged peptide system is closest to reality in the present work in terms of the Pi protonation state, the concentration ratios between Ca^{2+} and Pi, and the ionic strength (see below).

The initial helical backbone structure for the model peptide is generated based on the C-terminal helix of the human lymphotactin (NMR structure, PDB entry 1J9O), and the corresponding side chains are mutated to SpSpEEEEEEEE. For the case with unprotonated phosphorylated serines, which is closest to the physiological condition in our current study, 25 ns simulation is carried out, of which the last 24 ns has been used for data analysis. Three additional simulations with different initial Ca^{2+} and Pi configurations are performed up to 17 ns to check the generality of the template formation which is observed in the 25 ns simulation. The backbone atoms of the helix are subjected to a harmonic restraint with a force constant of 30 (kcal/mol)/Å^2 while the side chain atoms are allowed to move freely. For the unstructured conformation, a random coil structure is prepared by a high-temperature simulation, and all atoms are free of constraint during the productive simulations. Because of the high degree of flexibility of the random coil, significantly longer MD simulations (35 ns) and multiple initial peptide configurations (five simulations for each peptide charge state; each simulation is up to 5 ns) are sampled to better explore the conformational space.

2.1.2. Solution Environments. In the current work, Ca^{2+}, Pi (inorganic phosphate), Na^+ and Cl^- ions are added to the system to mimic the nucleation environment; details of the setup are summarized in Table 1. To be consistent with the −10 and −12 charge states of the phosphorylated peptide, Pi correspondingly is either $H_2PO_4^-$ or HPO_4^{2-}. Unfortunately, experimental measurement of the local concentrations for Ca^{2+} and Pi around the polyglutamic acid motifs of BSP during nucleation is not available. The current choice of Ca^{2+} concentrations is based on two considerations: (1) higher than the normal Ca^{2+} concentration in blood (2.25−2.75 mM)[63] to mimic supersaturation with respect to hydroxyapatite because the interactions between polyglutamic acid motifs and Ca^{2+} may result in an increased local concentration; (2) minimum concentration (or nearly minimum concentration for −12 charged peptide) of Ca^{2+} which may saturate all residue side chains of the studied peptides, e.g., 10 Ca^{2+} ions are added for the −10 charged peptide where one Ca^{2+} may coordinate with the side chain of one amino acid residue. Inorganic phosphate concentrations are prepared with the same two considerations as for Ca^{2+} ions. The ratio for Ca^{2+} and Pi concentrations is also varied. For example, for the −12 charged peptide system, HPO_4^{2-} is the inorganic phosphate, which is close to the phosphate component in the hydroxyapatite crystal (PO_4^{3-}). Earlier studies have indicated that the hypothetical "Posner's cluster" ($Ca_9(PO_4)_6$) may form the fundamental unit of an amorphous calcium phosphate phase that may transform to hydroxyapatite through the dissociation of Posner's cluster rather than undergoing complete ionic dissolution,[64−66] although this

(55) Rohl, C. A.; Strauss, C. E. M.; Misura, K. M. S.; Baker, D. *Method Enzymol.* **2004**, *383*, 66.
(56) Kim, D. E.; Chivian, D.; Baker, D. *Nucleic Acids Res.* **2004**, *32*, W526.
(57) Bradley, P.; Misura, K. M. S.; Baker, D. *Science* **2005**, *309*, 1868.
(58) Schueler-Furman, O.; Wang, C.; Bradley, P.; Misura, K.; Baker, D. *Science* **2005**, *310*, 638.
(59) Jones, D. T. *J. Mol. Biol.* **1999**, *292*, 195.
(60) He, G.; Ramachandran, A.; Dahl, T.; George, S.; Schultz, D.; Cookson, D.; Veis, A.; George, A. *J. Biol. Chem.* **2005**, *280*, 33109.
(61) Lee, S. L.; Glonek, T.; Glimcher, M. J. *Calcif. Tissue Int.* **1983**, *35*, 815.
(62) Glimcher, M. J. *Philos. Trans. R. Soc., London B* **1984**, *304*, 479.
(63) Committee on Minerals and Toxic Substances in Diets and Water for Animals, National Research Council. *Mineral Tolerance of Animals*, 2nd ed.; National Academies Press: Washington, DC, 1980.
(64) Betts, F.; Posner, A. S. *Mater. Res. Bull.* **1974**, *9*, 353.
(65) Posner, A. S.; Betts, F. *Acc. Chem. Res.* **1975**, *8*, 273.
(66) Yin, X. L.; Stott, M. J. *J. Chem. Phys.* **2003**, *118*, 3717.

Table 1. Simulation Setup for all Molecular Dynamics Calculations

system[a]			solution environments			
		name	number of water	number of ions	concentration of ions (M)[b]	simulation time (ns)[c]
α-helix	−10	pα10_Ca_Pi_NaCl	7673	10 Ca^{2+}, 10 $H_2PO_4^-$, 14 Na^+, 14 Cl^-	0.070 Ca^{2+}, 0.070 $H_2PO_4^-$, 0.098 Na^+, 0.098 Cl^-	5
	−12	pα12_Ca_Pi_NaCl	7656	18 Ca^{2+}, 12 HPO_4^{2-}, 14 Na^+, 14 Cl^-	0.125 Ca^{2+}, 0.084 HPO_4^{2-}, 0.098 Na^+, 0.098 Cl^-	25
random coil	−10	pr10_Ca_Pi_NaCl	7673	10 Ca^{2+}, 10 $H_2PO_4^-$, 14 Na^+, 14 Cl^-	0.070 Ca^{2+}, 0.070 $H_2PO_4^-$, 0.098 Na^+, 0.098 Cl^-	35
	−12	pr12_Ca_Pi_NaCl	7656	18 Ca^{2+}, 12 HPO_4^{2-}, 14 Na^+, 14 Cl^-	0.125 Ca^{2+}, 0.084 HPO_4^{2-}, 0.098 Na^+, 0.098 Cl^-	35
inorganic reference	−10	Ca_H_2PO_4_NaCl	7798	10 Ca^{2+}, 10 $H_2PO_4^-$, 14 Na^+, 24 Cl^-	0.070 Ca^{2+}, 0.070 $H_2PO_4^-$, 0.098 Na^+, 0.168 Cl^-	5
	−12	Ca_HPO_4_NaCl	7786	18 Ca^{2+}, 12 HPO_4^{2-}, 14 Na^+, 26 Cl^-	0.125 Ca^{2+}, 0.084 HPO_4^{2-}, 0.098 Na^+, 0.182 Cl^-	5

[a] The peptide conformation and charge state (unit: e) are used to label the different simulations; for the inorganic reference simulations, "-10" refers to the inorganic solution without the −10 e charged peptide, and "−12" refers to the inorganic solution without the −12 e charged peptide. [b] The concentration is calculated based on a cubic box with the side length of 62 Å. [c] The first nanosecond is used to equilibrate the system; for the random coil simulations, five additional simulations with different initial configurations are carried out for each charge state of the peptide (−10 e and −12 e), and every additional simulation is up to 5 ns.

idea has been criticized.[1] To investigate whether the Posner's cluster can form in the presence of the peptide, the ratio of Ca^{2+} and Pi concentrations is set to be 3:2. The concentration of NaCl is 0.1M, consistent with the normal salt condition in blood. To promote the interactions between Ca^{2+} and Pi with peptide, Ca^{2+} and Pi are initially at random positions near the peptide.

2.1.3. Reference Systems. Reference solutions with only inorganic ions (Ca^{2+}, Pi, Na^+, Cl^-) are investigated (without peptide) to make clear the effects of the peptide on the distribution of ions. Depending on the protonation state of Pi, two solution systems are studied. The concentrations of the Ca^{2+} and Pi in reference solutions are maintained to be the same as those in the corresponding peptide systems. Na^+ and Cl^- concentration are varied to keep the entire system charge neutral. The detailed setup is summarized in Table 1. Simulations of 5 ns are applied for reference systems.

2.2. Molecular Dynamics Simulations. Molecular dynamics simulations with periodic boundary conditions are carried out with the CHARMM program.[53,54] The CHARMM force field has been widely applied to study interactions between ions and protein/small molecules. Previous simulations showed reasonable consistence to the experimental results.[67−69] Partial charges and van der Waals parameters for HPO_4^{2-}, $H_2PO_4^-$, and Ca^{2+} are provided in the Supporting Information. An equilibrated cubic solvent box with the side length of 62 Å is used to solvate the peptide. For all simulations, the entire system includes about 23 600 atoms, and is charge neutral. The particle mesh Ewald method is used to treat electrostatic interactions.[70] For van der Waals interactions, a switching scheme[71] is applied for interatomic distances between 10 and 12 Å. Constant pressure and temperature simulations are carried out. The Nosé−Hoover algorithm[72,73] is used to control the system temperature to be 298 K, with a mass of 250 kcal·mol^{-1}.ps^2 for the thermostat. The Anderson algorithm[74,75] is applied to control the system pressure where the mass for the pressure piston is 500 amu, the reference pressure is 1 atm, the Langevin piston collision frequency is 10 ps^{-1}, and the Langevin piston bath temperature is 298 K. For all simulations, SHAKE[76] is applied to bonds involving hydrogen, which allows an integration time step of 2 fs; the first 1 ns simulation is used as equilibration and subsequent simulations are production runs for data collection.

To describe distributions of ions around the peptide, the running coordination numbers (integratedion−peptide-surface radial distribution function) for all ions are calculated for both the helical conformation and the random coil structure. The calculation method is adopted from Ma et al.'s work.[77] The shortest distances between a specific type of ion (Ca^{2+}, Pi, Na^+, Cl^-) and the peptide atoms are collected from MD simulation trajectories. For Pi, the phosphorus atom is used in the distance measurement. For more details, please refer to ref 77.

3. Results

3.1. Peptide in α-Helical Conformation. *Interactions among Ca^{2+}, Pi, and Peptide Side Chains.* During the simulation, Ca^{2+} ions form direct and persistent interactions with the acidic side chains of the peptide through electrostatic interactions. For example, for both pα10_Ca_Pi_NaCl and pα12_Ca_Pi_NaCl simulations, the running coordination number of Ca^{2+} ions around the peptide indicates that all Ca^{2+} ions are proximate to the peptide (Figure 1). For both peptide models, at the time scale of the simulation, no exchange of the Ca^{2+} ions bound to different peptide side chains is observed. Peptide side chains directly and strongly localize Ca^{2+} ions through electrostatic interactions (Figure 1). For the pα10_Ca_Pi_NaCl system, each residue side chain has only one Ca^{2+} to coordinate. The carboxylate group of Glu residue binds each Ca^{2+} ion in a bidentate fashion with the two unprotonated oxygen atoms (Oε1 and Oε2). The deprotonated oxygen of the Ser-phosphate group binds Ca^{2+} in a monodentate mode. The interaction between Ca^{2+} ions and the peptide in the pα12_Ca_Pi_NaCl system is illustrated in Figure 2. In the pα12_Ca_Pi_NaCl system, due to the excess Ca^{2+} ions (18 Ca^{2+}) compared to the number of side chains (10), each residue side chain can coordinate at least one Ca^{2+} and potentially multiple Ca^{2+} ions through electrostatic interactions with Pi, thus forming a Ca−Pi cluster. For example, two to three Ca^{2+} ions and Pi coordinate with each Ser-phosphate around the N-terminus of the peptide (Figure 2).

Pi forms extensive networks with Ca^{2+} ions around the peptide, and phosphate motifs of the phosphorylated Ser can be part of the Ca^{2+}−Pi networks (Figure 2 and 3) independent of the phosphate protonation states. Each Pi may interact with up to four Ca^{2+} ions. In this way, neighboring Ca^{2+} ions in space are bridged by Pi, resulting in a compact and stable Ca^{2+} ion distribution pattern.

As expected, Pi does not directly interact with the side chains of the peptide due to electrostatic repulsion (Figures 2 and 3). For both the pα10_Ca_Pi_NaCl and pα12_Ca_Pi_NaCl systems, the

(67) Potoff, J. J.; Issa, Z.; Manke, C. W.; Jena, B. P. *Cell Biol. Int.* **2008**, *32*, 361.
(68) Allen, T. W.; Andersen, O. S.; Roux, B. *Proc. Natl. Acad. Sci. U.S.A.* **2004**, *101*, 117.
(69) Bastug, T.; Kuyucak, S. *Chem. Phys. Lett.* **2006**, *424*, 82.
(70) Darden, T.; York, D.; Pedersen, L. *J. Chem. Phys.* **1993**, *98*, 10089.
(71) Steinbach, P. J.; Brooks, B. R. *J. Comput. Chem.* **1994**, *15*, 667.
(72) Nose, S. *J. Chem. Phys.* **1984**, *81*, 511.
(73) Hoover, W. G. *Phys. Rev. A* **1985**, *31*, 1695.
(74) Feller, S. E.; Zhang, Y. H.; Pastor, R. W.; Brooks, B. R. *J. Chem. Phys.* **1995**, *103*, 4613.
(75) Andersen, H. C. *J. Chem. Phys.* **1980**, *72*, 2384.
(76) Ryckaert, J. P.; Ciccotti, G.; Berendsen, H. J. C. *J. Comput. Phys.* **1977**, *23*, 327.
(77) Ma, L.; Cui, Q. *Biochemistry* **2006**, *45*, 14466.

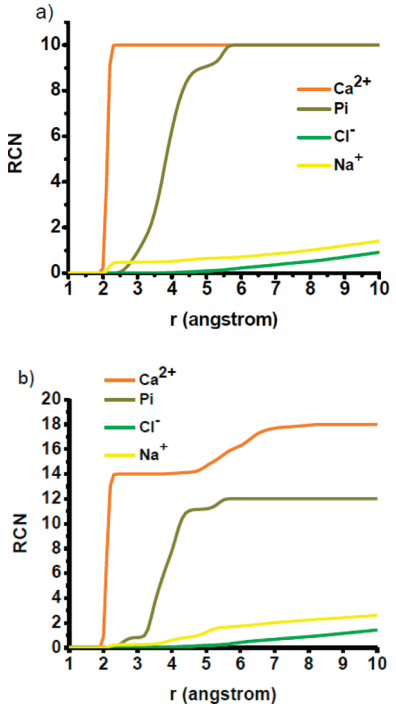

Figure 1. Running coordination number (RCN) for different ions around the peptide for the (a) pα10_Ca_Pi_NaCl and (b) pα12_Ca_Pi_NaCl systems. The distribution is measured relative to the peptide surface as in ref 77. For Pi, the phosphorus atom is used for distance measurement.

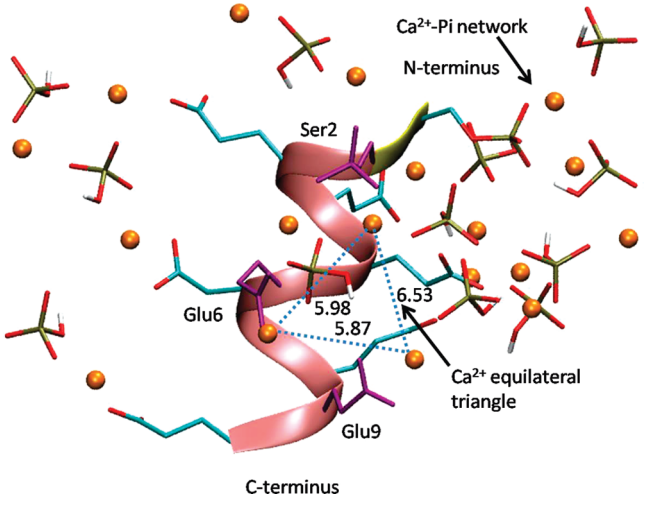

Figure 2. Snapshot illustrating the interactions among Ca^{2+}, Pi, and the peptide in the pα12_Ca_Pi_NaCl simulation. The peptide backbone is rendered in ribbons; Ser residues are in yellow and Glu residues are in dark pink. The heavy atoms of the peptide side chains are represented in licorice, with oxygen in red, carbon in cyan and phosphorus in tan. Ca^{2+} ions are in orange and the CPK representation. Pi are in the licorice representation, with hydrogen atoms in white. Ser2, Glu6, and Glu9, which coordinate three Ca^{2+} ions in an equilateral triangle (indicated with blue dotted lines, distances in Å), are highlighted in purple.

distribution of Pi−peptide distances along the production trajectory peaks around 3.5−4.2 Å. The present observation is consistent with earlier ^{31}P NMR experiments that studied ternary complex formation of fetal calf dentin phosphoprotein with calcium and inorganic orthophosphate ions.[61,62] Addition of $CaCl_2$ to the solution containing both the phosphoprotein and

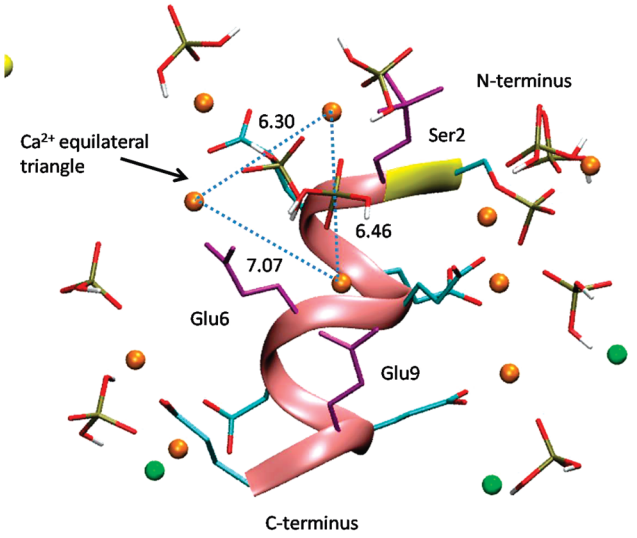

Figure 3. A snapshot that illustrates the interactions among Ca^{2+}, Pi, and the peptide in the pα10_Ca_Pi_NaCl simulations. See Figure 2 for the color and representation schemes.

inorganic orthophosphate ions broadened or obliterated the phosphomonoester peak and the inorganic orthophosphate peak, but such a broadening was not observed when $CaCl_2$ is absent. The interpretation is that inorganic orthophosphate ions bind to Ca^{2+} associated with the phosphoprotein and stable Ca^{2+}−Pi networks are formed around the peptide, such that both phosphomonoester and inorganic orthophosphate NMR peaks are affected.

The background electrolyte ions, Na^+ and Cl^-, do not form stable interactions with the complex formed by Ca^{2+}, Pi, and the peptide. On average, only one to two Na^+/Cl^- ions are present within 10 Å from the peptide (Figure 1). Na^+ and Cl^- ions may diffuse close to the complex and form transient interactions, but do not significantly perturb interactions among Ca^{2+}, Pi, and the peptide.

Ca^{2+} Equilateral Triangle. An interesting observation for both pα10(12)_Ca_Pi_NaCl systems in some of the simulations is that around the N-terminus of the peptide, three Ca^{2+} ions form an equilateral triangle through the Ca^{2+}−Pi networks. Representative triangular structures are shown in Figure 2 and 3. The Ca^{2+} ions coordinate with the Ser2, Glu6, and Glu9 side chains. Figure 4 shows the detailed analyses for the Ca^{2+} equilateral triangle from both systems. For pα12_Ca_Pi_NaCl, the Ca^{2+} triangle coordinated with Ser2, Glu6, and Glu9 converges to a stable equilateral geometry within the entire 25 ns simulation. For example, for the last 16 ns simulation, the average distances for Ca^{2+}(Ser2)−Ca^{2+}(Glu6), Ca^{2+}(Ser2)−Ca^{2+}(Glu9), and Ca^{2+}-(Glu6)−Ca^{2+}(Glu9), respectively, are 5.98, 6.53, and 5.87 Å, with fluctuations of 0.12, 0.26, and 0.26 Å, respectively. The average circumference for the Ca^{2+} triangle is 18.38 Å with a fluctuation of 0.48 Å. The pattern of the Ca^{2+} equilateral triangle coordinated with peptide side chains is similar to a Ca^{2+} equilateral triangle on the (001) surface of the hydroxyapatite crystal, where the Ca^{2+}−Ca^{2+} distance is 6.15 Å and the corresponding circumference is 18.45 Å. We compared the Ca^{2+}−P triangle formed in our simulation to triangular atom arrangement on the other faces of the hydroxyapatite crystal (including the (010), (100), (110) faces), but we did not find apparent matching patterns on any other hydroxyapatite faces. The Ca^{2+} equilateral triangle is largely stabilized by interactions with Pi in the Ca^{2+}−Pi networks as discussed earlier, where each Pi bridges two neighboring Ca^{2+}

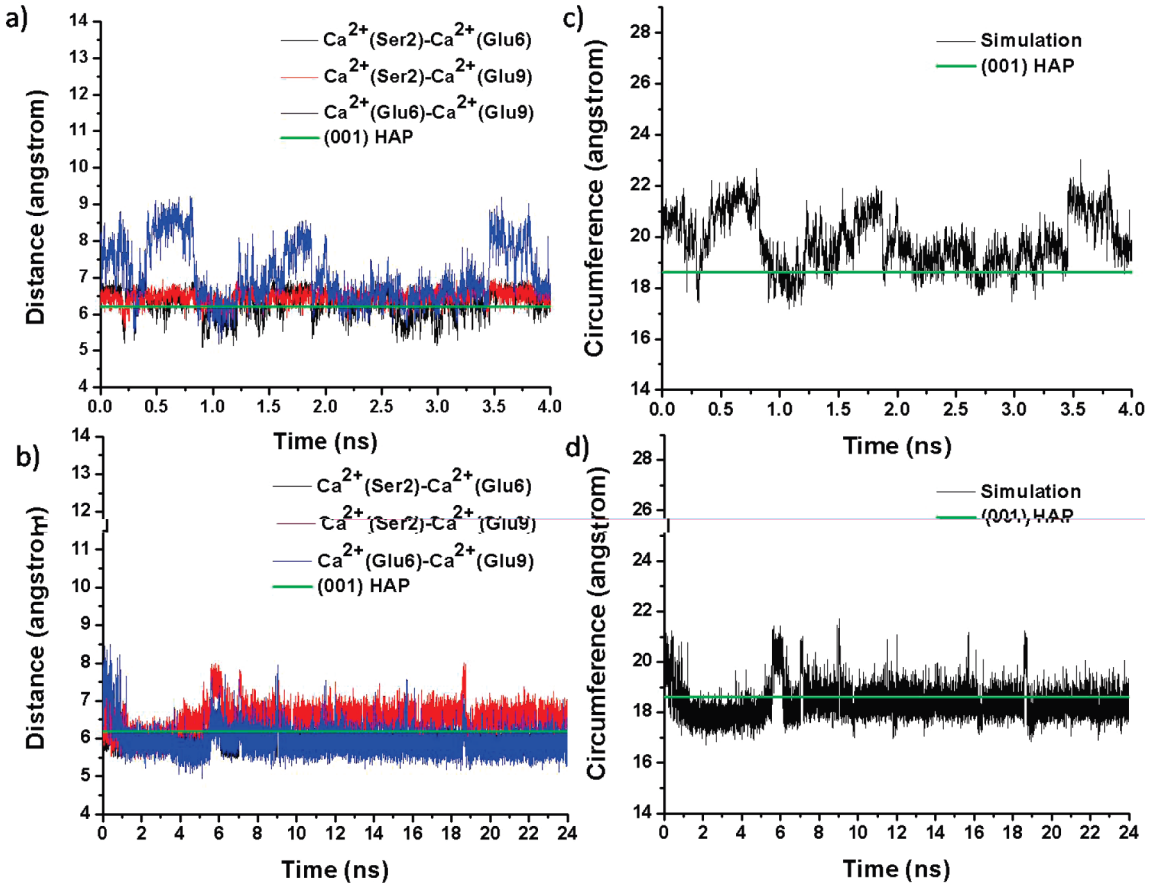

Figure 4. Side lengths (a, b) and circumference (c, d) for the Ca^{2+} equilateral triangle formed with Ser2, Glu6, and Glu9 in the pα10_Ca_Pi_NaCl (a, c) and pα12_Ca_Pi_NaCl (b, d) simulations. The green line indicates the corresponding value for the (001) surface of the hydroxyapatite crystal.

ions through the deprotonated oxygen atoms. Thus, it appears that formation of the Ca^{2+} triangle requires not only the spatial arrangement of the peptide side chains but also the involvement of the Pi to generate stable interaction networks. We note that the ~6 Å equilateral triangle templated by the α-helical conformation also matches Ca^{2+} ion spacing on the (001) face of the octacalcium phosphate. Therefore, in all the following discussions, where we speak of templating (001) face of hydroxyapatite, the arguments would also be valid for the (001) face of the octacalcium phosphate. We note, however, that the crystal structure of the octacalcium phosphate may be viewed as two unit cells of the hydroxyapatite with a layer of water between them. Therefore, on the nanoscale of the earliest nucleated calcium phosphate crystals, it may be difficult to distinguish empirically between the hydroxyapatite and the octacalcium phosphate.

Compared to the pα10_Ca_Pi_NaCl system, more Ca^{2+} equilateral triangles could be formed in the pα12_Ca_Pi_NaCl system due to the higher concentration of Ca^{2+}. However, the triangle is not stable and breaks apart as the simulation proceedings for longer periods. For example, one Ca^{2+} triangle coordinated with Ser1, Glu5, and Glu8 gradually forms after 1.5 ns simulation (Figure 5), and is stable for the following 2.5 ns of simulation with the average distances for Ca^{2+}(Ser1)−Ca^{2+}(Glu5), Ca^{2+}(Ser1)−Ca^{2+}(Glu8) and Ca^{2+}(Glu5)−Ca^{2+}(Glu8) of 6.35, 6.48, and 5.86 Å, respectively, and with fluctuations of 0.33, 0.34, and 0.15 Å, respectively. The average circumference for the Ca^{2+} triangle is 18.69 Å with a fluctuation of 0.48 Å. This resulting pattern of the Ca^{2+}, again, matches the equilateral triangle of Ca^{2+} ions on the (001) surface of the hydroxyapatite crystal. Nevertheless, after 4 ns, the side lengths of the triangle start to diverge, and the equilateral triangle does not form again subsequently.

Considering the limit of the current simulation length, three additional simulations up to over 17 ns with different initial Ca^{2+} and Pi configurations for the pα12_Ca_Pi_NaCl system were performed to probe the generality of the formation of the Ca^{2+} equilateral triangle. It turned out that only one of the three simulations gave a stable Ca^{2+} equilateral triangle formed by Ser2, Glu6, and Glu9 up to 17 ns, and in all of the three simulations, no Ca^{2+} equilateral triangle was formed with Ser1, Glu5, and Glu8. Please see the detailed structural analyses in the Supporting Information (Figure S1). The additional simulations indicate that, although Ca^{2+} equilateral triangle may form from some starting ion distributions due to conformations of the specific side chains of the helical peptide, the formation is not universal.

Despite the above caveat, it is important to point out that the match in structure of the Ca^{2+} equilateral triangle associated with the peptide and the Ca^{2+} ions on the (001) face of hydroxyapatite suggests a possible template for a direct induction of the crystalline hydroxyapatite nucleation. At least, through simulations, we observe that the side chains of the peptide in the helical conformation have the potential to facilitate the Ca^{2+} equilateral triangle formation with their specific spatial arrangement. For example, to form a stable Ca^{2+} equilateral triangle template, three amino acids are needed. For the two Ca^{2+} equilateral triangles observed around the peptide N-terminus in the 25 ns simulation, residues Ser2, Glu6, Glu9 and Ser1, Glu5, Glu8 are involved. It is

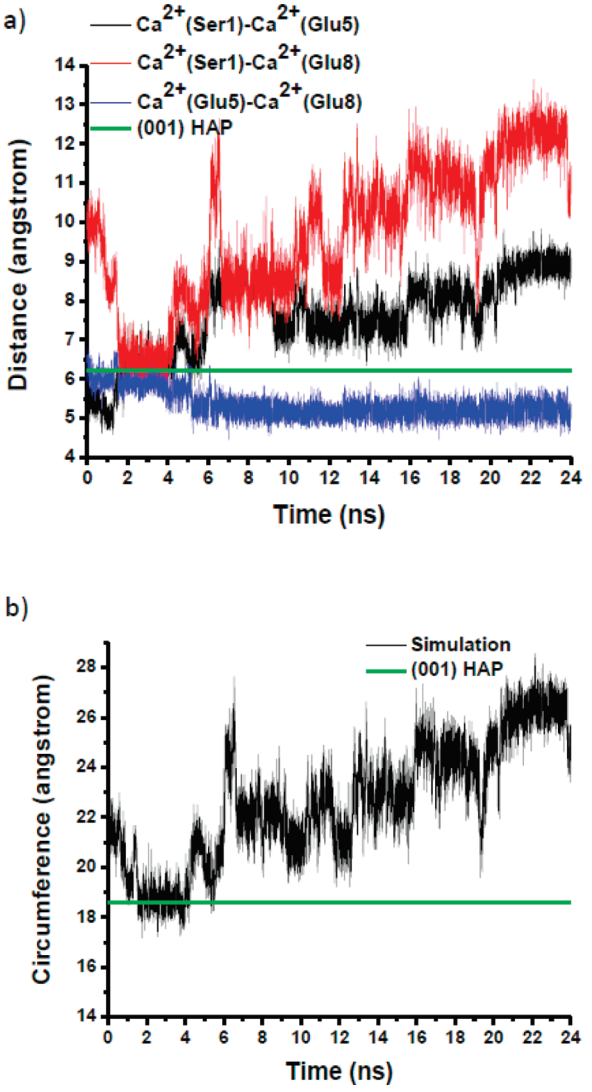

Figure 5. Side lengths (a) and circumference (b) for the unstable Ca^{2+} equilateral triangle formed with Ser1, Glu5, and Glu8 in the pα12_Ca_Pi_NaCl simulation. The green line indicates the corresponding value for the (001) surface of the hydroxyapatite crystal.

interesting to note that both sets of residues show the same side chain separation pattern, i.e., $n, n+4, n+7$, where n is the residue index in the model peptide. In other words, the spatial arrangement of residues $n, n+4$, and $n+7$ in an α-helix might be ideal for arranging Ca^{2+} to form an equilateral triangle pattern. The presence of a nucleating site on BSP that consists of one phosphorylated Ser and two Glu residues has been proposed previously base on *ab initio* calculations.[41] The present observation may partially explain the experimental observation by Tye et al. that a sequence of at least eight contiguous glutamic acid residues is required for the nucleation of hydroxyapatite by BSP.[12] Interestingly, however, those authors claimed that the nucleating "site" is not α-helical in conformation. In summary, we reiterate that the observed side chain pattern templating the triangular Ca^{2+} cluster provides just one possibility.

Comparisons with Reference Simulations—Solutions with Inorganic Ions. To examine the role of the peptide on nucleation, systems involving inorganic ions only without the peptide are studied, and the concentrations of the inorganic ionic species are kept the same as for the corresponding peptide systems discussed above. These inorganic systems are labeled as Ca_H_2PO_4_NaCl and Ca_HPO_4_NaCl, referring to the different phosphate protonation states.

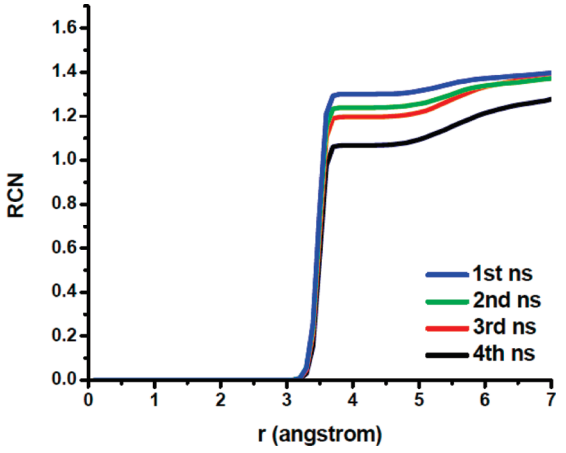

Figure 6. Running coordination number (RCN) for Ca^{2+} ions around Pi (phosphorus atom is used in calculations.) at different stages of the simulation for the inorganic solution system Ca_H_2PO_4_NaCl.

Simulations of the reference systems indicate that calcium phosphate clusters may form independent of the Pi protonation state. In sharp contrast to the peptide systems; however, not only the geometry of the formed clusters fluctuates but also the identities of the ions in the cluster may vary. For example, a single Pi ion may diffuse and electrostatically interact with an existing cluster and form a larger cluster. To characterize these features, Pi distance matrix and Ca^{2+} distance matrix are generated for both reference systems to show the dynamic features along the simulation (Supporting Information Figure S2 and S3; see the Supporting Information for the calculation method). Small clusters are formed in the Ca_H_2PO_4_NaCl system, where two Pi's interact with each other through one or two Ca^{2+} ions, and the clusters remain stable throughout the 4 ns simulation. For example, during the first nanosecond, Pi 2 and 6 form a cluster and Pi 9 and 10 form a cluster, and these clusters are present for the entire trajectory. In addition, new clusters are formed throughout the simulations. For example, in the fourth nanosecond, Pi 4 and 5 form a cluster, which is not observed in the earlier part of the trajectory. Also, the distance between Pi 2 and 6 becomes shorter along the simulation trajectory, which indicates that the cluster becomes more aggregated (Figure S2). The running coordination number (RCN) for Ca^{2+} ions around Pi (phosphorus atom is used in calculations) shown in Figure 6 also indicates the Ca^{2+}−Pi aggregation as the simulation proceeds. For example, there are, on average, 1.1 Ca^{2+} ions within 4.5 Å from Pi in the first nanosecond; this value gradually increases to 1.3 in the fourth nanosecond.

Even though the cluster components are spatially close, the cluster may adopt dramatically different conformations throughout the simulation. For instance, either one or two Ca^{2+} ions may be shared by two Pi, and also each Pi may rotate in the cluster formed by Pi 9 and 10 and Ca^{2+} 1 and 5 in the system of Ca_H_2PO_4_NaCl. Figure 7 shows the rmsd for this cluster and representative conformations during the simulation. Compared to the Ca^{2+}−Pi networks formed in the corresponding peptide system, the cluster formed in the inorganic system is much less ordered. This observation is consistent with the result of MD simulations of Ca^{2+}−dimethylphosphate (DMP^-) complex formation by Potoff et al., who studied Ca^{2+} mediated local dehydration of Ca^{2+} ions and membrane phosphate head groups,

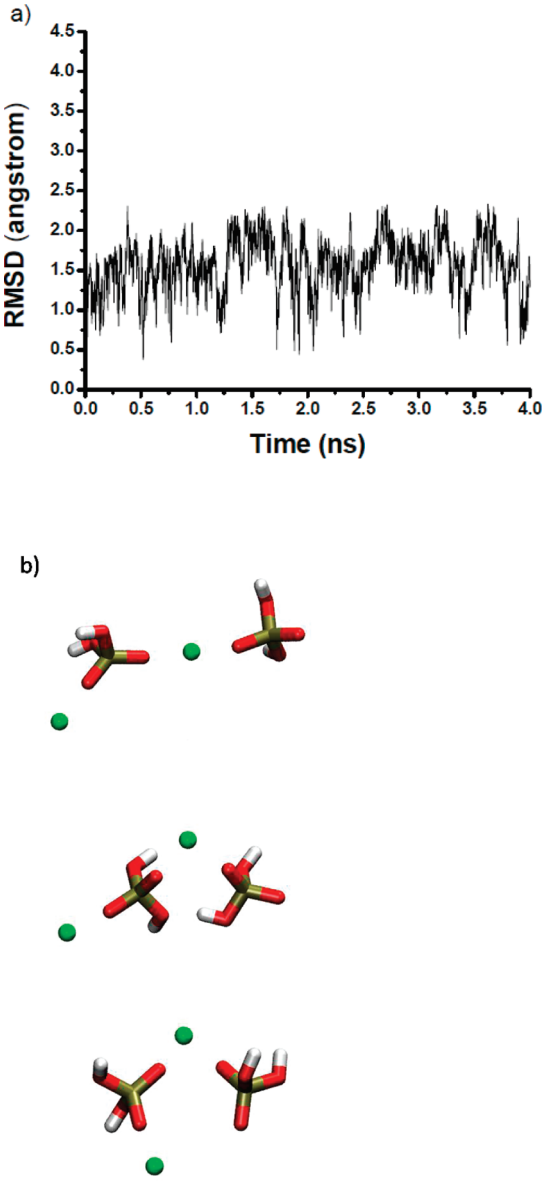

Figure 7. Root-mean-square-deviation (rmsd) (a) for the cluster formed by phosphate 9 and 10 and Ca^{2+} 1 and 5 in the inorganic solution system of Ca_H_2PO_4_NaCl. Representative structures are shown in part b.

and membrane fusion in cells.[67] For an aqueous solution of Ca^{2+} (0.3 M) and DMP^- (0.6 M), two Ca^{2+} ions can bridge two DMP^- molecules by binding to the anionic oxygens of the DMP^- molecule, resulting in the formation of a ring-like structure. Besides the ring conformation, linear and bent complexes were also observed when a single Ca^{2+} cation bridged two DMP^- molecules. In our study, the largest stable cluster observed in the Ca_H_2PO_4_NaCl system includes two Ca^{2+} and two Pi. No apparent matching pattern to the crystal structure is observed.

In the Ca_HPO_4_NaCl system (Supporting Information; Figure S4 and S5 show distance matrices), our simulations result in more extensive cluster formation compared to the Ca_H_2PO_4_NaCl system, which is consistent with expectation since Pi is only singly protonated and the concentrations of Ca^{2+} and Pi are higher than those in the Ca_H_2PO_4_NaCl system. As a dramatic example, there are five phosphate ions surrounding phosphate 8 with distance separations of less than 8.0 Å in the fourth nanosecond, which implies that a complicated and large structure is formed. Also,

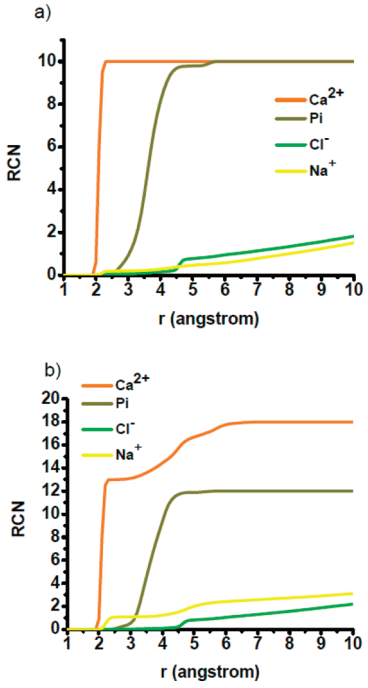

Figure 8. Running coordination number (RCN) for different ions around the peptide surface for the systems of pr10_Ca_Pi_NaCl (a) and pr12_Ca_Pi_NaCl (b). The distribution is measured relative to the peptide surface as in ref 77. For Pi, the phosphorus atom is used for distance measurement.

throughout the simulation, the cluster components vary and phosphate tends to aggregate and form larger clusters. For example, from the first to the fourth nanosecond, the number of P−P distances within 8.0 Å increases from 13 to 17. Representative structures for clusters are shown in Supporting Information, Figure S6. The largest stable cluster in this case includes 7 Pi and 11 Ca^{2+} ions with the longest cluster dimension of around 1.5−2 nm. Although the cluster structure experiences significant fluctuation, and does not provide a template for the hydroxyapatite crystal, it may serve as a nucleation center for amorphous calcium phosphate precipitation. This observation is consistent with nucleation from solution supersaturated with respect to hydroxyapatite.

3.2. Peptide in Random Coil Structure. To probe conformational effect of the peptide on the ion distribution in solution, we study two protonation states of the peptides in a random coil structure, namely pr10_Ca_Pi_NaCl and pr12_Ca_Pi_NaCl.

Figure 8 shows the running coordination numbers of ions around the peptide, and the results are largely similar to those with the helical peptide. Similar to the helical peptide systems, Ca^{2+} ions directly interact with the random coil peptide side chains. Some of the Ca^{2+} ions, however, are shared by side chains of spatially nearby residues. Na^+ and Cl^- ions diffuse in bulk solution and most of them do not form stable interactions with the peptide or Ca^{2+}−Pi networks. Thus, Na^+ and Cl^- ions do not directly affect the Ca^{2+}/Pi−peptide interactions. Also similar to the helical peptide, Pi form indirect interactions with the peptide through Ca^{2+}−Pi networks. In contrast to the helical conformation, no Ca^{2+} equilateral triangle is observed for the pr10_Ca_Pi_NaCl system despite the formation of Ca^{2+}−Pi networks associated with the peptide. For the pr12_Ca_Pi_NaCl system, an approximately equilateral triangle of Ca^{2+} is formed at ~2.3 ns into the production run (Figure 9). The average distances for Ca^{2+}(Glu8, Glu9)−Ca^{2+}(Glu6), Ca^{2+}(Glu8, Glu9)−Ca^{2+}(Glu5, Glu6), and Ca^{2+}(Glu5, Glu6)−Ca^{2+}(Glu6) are 5.75, 5.48, and 4.94 Å,

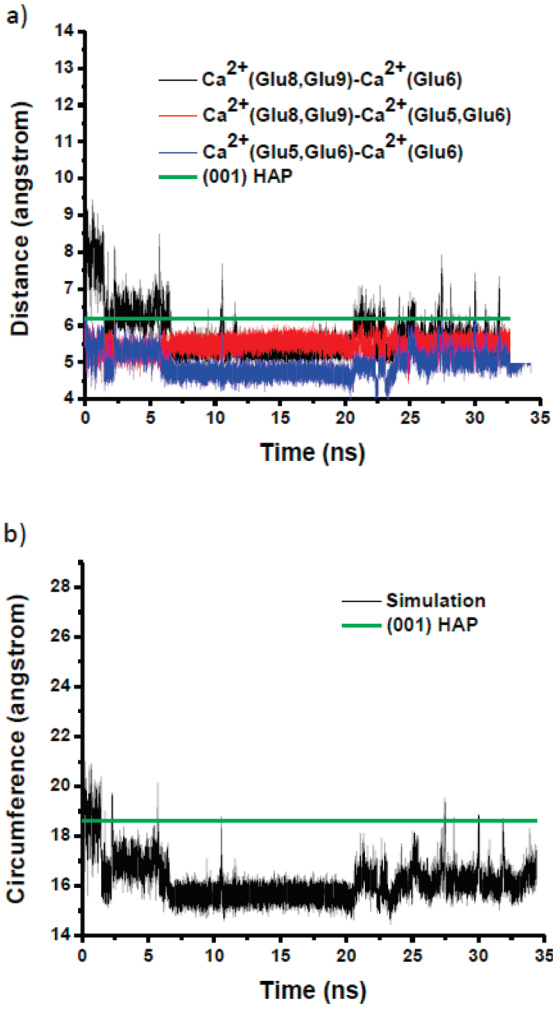

Figure 9. Side lengths (a) and circumference (b) for the most apparent Ca^{2+} equilateral triangle observed in the pr12_Ca_Pi_NaCl simulation. The green line indicates the corresponding value for the (001) surface of the hydroxyapatite crystal.

respectively, with fluctuations of 0.62, 0.20, and 0.32 Å, respectively. The average circumference is 16.17 Å and the associated fluctuation is 0.82 Å. The values indicate a less optimal equilateral triangle compared to the helix case. Two of the three Ca^{2+} ions are shared by side chains, but the host side chains do not follow the *n*, *n*+4, *n*+7 pattern observed for the helical peptide system. During the nanosecond-scale simulations, no Ca^{2+} ions or Pi diffuse into the bulk solution, similar to the helical peptide system.

Starting from different initial configurations, additional simulations (for 5 ns each) are performed for the peptide in both charge states. For the pr10_Ca_Pi_NaCl system, no Ca^{2+} triangle template is observed in any of the 5 additional simulations, and no Ca^{2+} triangle template is observed in three of the additional simulations for the pr12_Ca_Pi_NaCl system. However, a Ca^{2+} equilateral triangle is observed in two simulations of the pr12_Ca_Pi_NaCl system, where two Ca^{2+} ions coordinate with the Ser2 phosphate and the third Ca^{2+} coordinates with the Glu3 side chain. The formed triangle is less optimum than the one from the helical conformation. For example, the average lengths of the three sides of the Ca^{2+} triangle are 4.96, 6.25, and 5.31 Å, respectively, with fluctuations of 0.41, 0.81, and 0.29 Å, respectively. The average circumference is 16.52 Å and the associated fluctuation is 1.19 Å. This triangle formation scheme is also different from the one observed in the 35 ns simulation of the

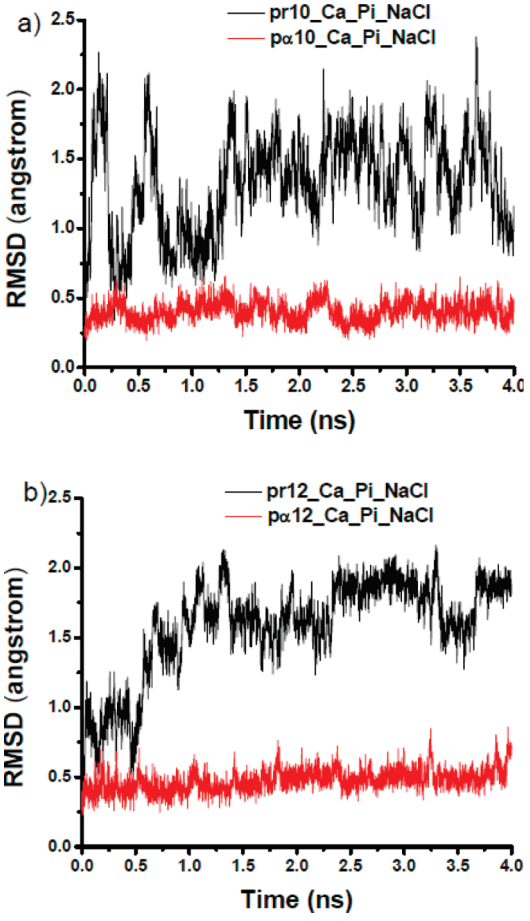

Figure 10. Root-mean-square-deviation (rmsd) for backbone atoms of the peptide in the helical conformation and the random coil structure: (a) for the p10 system; (b) for the p12 system. Note that the helical conformation is not subjected to any constraints during the simulations that produced the rmsd values in this figure.

pr12_Ca_Pi_NaCl system, in which one Ca^{2+} ion is associated with Glu8 and Glu9, another with Glu6, and the third Ca^{2+} with Glu5 and Glu6. It appears that although the Ca^{2+} triangle occasionally forms, there is no specific trend in side chain involvement, and the triangle formation appears to be random.

For both systems, the peptide in random coil shows significant structural fluctuations. Figure 10 shows the rmsd for the backbone atoms during the simulations. To provide a systemic comparison, nonrestrained simulations with the peptide in α-helical conformation are carried out. Clearly, under the respective ion concentrations, the α-helical conformation is stable independent of its charge state. In addition, as expected, the solvent accessible surface area (SASA) for the random coil structure is significantly larger than that of the respective helical conformation for both peptide protonation states (Figure S7 in the Supporting Information). The simulations clearly highlight that the random coil is structurally more flexible and extensive than the helical conformation.

4. Discussions

We begin the discussion with a reminder that our present work tries to probe how the residue side chains of the peptide in different conformations control the ion distributions in solution, which, in principle, is the first step for a heterogeneous nucleation process. To achieve the goal, we performed an effective accelerated simulation. For example, in our simulations, Ca^{2+} and Pi are initially at random positions near the peptide. In this way, we

skipped the initial ion diffusion process from bulk solution to a location close the peptide surface. Second, as indicated above, the concentrations of Ca^{2+} and Pi in our simulation are all larger than those in the blood to mimic supersaturation with respect to hydroxyapatite, so our system should have a shorter induction time than the real system. Finally, for the simulations of the helical conformation, during the whole simulation, the peptide backbone atoms are restrained with a harmonic potential. Thus, large structure variations are avoided and the numbers of variables that affect theion−peptide interactions are minimized. On the basis of the conditions prepared, the peptide side chain conformational change and its interaction with ions becomes a relatively short-time-scale event, which could be addressed by the present MD simulation.

The acidic motif of BSP could influence the nucleation process. Comparison of peptide structure simulations reveals that occasionally the helical conformation adopts side chains positions that promote Ca^{2+} ion distributions to match those in the (001) surface of the hydroxyapatite crystal. Thus, the possibility of the helical conformation to induce orientated hydroxyapatite nucleation by forming a crystal matching template is shown to exist. Because of the limit of the time scale of the present simulation work; however, it is difficult to prove definitively whether the observed template is robust and unique in reality. In fact, for both the helical conformation and random coil structure, we do not observe apparent template formation in most of the simulations; most importantly, the triangular template is observed to break up in the pα12_Ca_Pi_NaCl system after 4 ns. These results seem to imply that independent of peptide conformations, the BSP nucleating motif (i.e., the 10-mer peptide) is likely to help nucleate amorphous calcium phosphate cluster, which ultimately converts to crystalline hydroxyapatite. The amorphous precursor may be formed by the promotion of local supersaturation by the peptide in either conformation. Each of these possibilities is examined below in terms of their physical chemistry and the experimental evidence, or lack thereof.

For promoting nucleation, the acidic motif of BSP (SpSpEEEEEEEE) may function in several ways. On the basis of the classical nucleation theory and using a spherical nucleus as an example, the activation free energy for homogeneous nucleation is

$$\Delta G_N = \frac{16\pi\sigma^3 v^2}{3(kT\ln\Omega)^2}$$

where σ is the solid−liquid interfacial free energy per unit surface area (or interfacial tension, and assumed to be independent of cluster size), v is the molecular volume, k is the Boltzmann constant, T is temperature, Ω is the relative supersaturation defined as IAP/K_{sp}, where IAP refers to ion activity product and K_{sp} is the solubility product. To promote nucleation, the activation free energy barrier needs to be lowered. Because of the anionic nature of the nucleating motif, BSP attracts Ca^{2+} ions in solution (further coupled with Pi) resulting in increased local concentrations for both Ca^{2+} and Pi in the proximity of the protein. The aggregation of Ca^{2+} and Pi around the protein surface effectively increases the local Ω, thus decreasing the free energy barrier. According to the present simulations, both the helical conformation and random coil structure help to increase the local Ω. It is expected that the random coil structure is more efficient in increasing Ω because of its more dynamic nature. For example, in the inorganic Ca_H_2PO_4_NaCl reference solution, the largest stable Ca^{2+}−Pi cluster contains 2 Ca^{2+} ions and 2 Pi, and the helical peptide system pα10_Ca_Pi_NaCl attracts only a slightly larger cluster of 3 Ca^{2+} and 3 Pi; in comparison, the largest cluster extends significantly to involve 6−7 Ca^{2+} and Pi in the random coil system of pr10_Ca_Pi_NaCl. However, this effect becomes less pronounced for the Ca_HPO_4_NaCl and p12 systems, due to the increased Ca^{2+} and Pi concentrations and deprotonation of Pi. For example, the largest stable cluster includes 11 Ca^{2+} and 7 Pi in the inorganic reference solution, similar to 13 Ca^{2+} and 8 Pi ions for the pα12 system and 12−13 Ca^{2+} and 7−8 Pi ions for the pr12 system. We note that the p12 system is closer to the physiological condition, so the effect of increasing local Ω by either the random coil structure or the helical structure is not significant compared to the inorganic solution. Furthermore, although increasing Ω decreases ΔG_N, increasing the local ion activity is not an efficient way to promote nucleation due to the $(\ln\Omega)^{-2}$ dependence of ΔG_N.

Although the formation of the nucleating template is not general and frequent from the present simulations, it is necessary for us to discuss the possible direct induction of the orientated hydroxyapatite, since once the template is formed, the subsequent nucleation proceeds in a relatively easy manner. For example, since ΔG_N depends steeply on the interfacial energy of the molecular aggregate ($\Delta G_N \sim \sigma^3$), a small perturbation on σ may cause a significant effect on the nucleation rate. Thus, compared to increasing Ω, reducing σ is a much more effective way to lower the nucleation free energy barrier. Because of the strong electrostatic interactions with Ca^{2+} and possible proper spacing of side chains, the nucleating motif of BSP in the helical conformation induces the formation of Ca^{2+}−Pi clusters around the protein, in which the Ca^{2+} equilateral triangle matches the (001) hydroxyapatite structure. Because of the 2-D template, the interfacial energy between the Ca^{2+} equilateral triangle and the nucleating cluster will be smaller than that between the cluster and the solution. Thus, the nucleation of the orientated hydroxyapatite is promoted by lowering the interfacial energy. It is possible that the helical conformation is capable of nucleating the orientated hydroxypaptite in this more efficient way. However, due to the infrequent formation of the template, the significance of such effects of the helical conformation could be significantly compromised.

Taking into account all the above considerations, including the effects of peptide structures on Ω and σ, it appears that due to the electrostatic attraction, BSP nucleating motif may induce the increase of the relative supersaturation around the peptide surface, thus precipitation of a calcium phosphate phase is promoted. For most of our simulations, no apparent matching template to the hydroxyapatite crystal lattice is observed independent of peptide conformations. Thus, in those cases, nucleation of the amorphous calcium phosphate is facilitated. However, occasionally, the formation of Ca^{2+} equilateral triangle, which matches the Ca^{2+} ion distribution along the (001) surface of the hydroxyapatite, is observed with the peptide in the helical conformation, and nucleation of the orientated hydroxyapatite may be promoted through lowering the interfacial energy. But considering that the template formation is not consistently shown in our simulations, the templating effect with the helical conformation is not likely to be the dominant mechanism.

In fact, it has been a long-standing debate whether the vertebrate mineralization is initiated with the first deposit of an amorphous disordered mineral precursor.[62,78−83] Results of many

(78) Termine, J. D.; Posner, A. S. *Science* **1966**, *153*, 1523.
(79) Termine, J. D.; Posner, A. S. *Nature* **1966**, *211*, 268.
(80) Brown, W. E.; Chow, L. C. *Annu. Rev. Mater. Sci.* **1976**, *6*, 213.
(81) Weiner, S. *Bone* **2006**, *39*, 431.
(82) Grynpas, M. D. *Bone* **2007**, *41*, 162.
(83) Crane, N. J.; Popescu, V.; Morris, M. D.; Steenhuis, P.; Ignelzi, M. A. *Bone* **2006**, *39*, 434.

experimental studies have supported the notion that the amorphous calcium phosphate phase is the first-formed phase in the vertebrate bone formation. For example, using infrared spectroscopy, Lowenstam and co-workers demonstrated that the initial precipitate of a biologically formed calcium phosphate mineral is amorphous when studying the chiton teeth.[84] Mahamid et al. found an abundant amorphous calcium phosphate phase is present in the newly formed fin bones, when using the continuously growing fin bony rays of the Tuebingen long-fin zebrafish as a model for bone mineralization.[85] With Raman spectroscopy, Crane et al. obtained the evidence of amorphous calcium phosphate during intramembranous mineralization in matrix vesicle, although the observed mechanism might not be same as that for the bone formation in the extracellular environment.[83] In addition, when studying the dentin matrix protein **1** (DMP1, an acidic protein similar to BSP, where four acidic clusters were identified in the functional domain) mediated hydroxyapatite nucleatoin *in vitro*, amorphous calcium phosphate precipitates were shown by scanning electron microscope. Very recently, Yang et al. showed that amelogenin (an extracellular matrix protein found in developing tooth enamel) forms stable interactions with amorphous calcium phosphate at the early stages of hydroxyapatite formation.[86] Similar to the biomineralization of hydroxyapatite, recent experimental work also suggests the formation of an amorphous $CaCO_3$ precursor, that transforms to aragonite in mollusk shell nacre[87] and to calcite in sea urchin spine.[88−92] Therefore, although to our knowledge, the characterization of the first calcium phosphate nucleation phase induced by BSP is not available to date, our present inference that independent of peptide conformations, BSP nucleating motif is more likely to help nucleate amorphous calcium phosphate that ultimately transforms to hydroxyapatite crystal is consistent to other similar biomineralization systems.

As an interesting point to note, although the concept of structural pattern matching (templating) for promoting nucleation was popular in the biomineralization field,[93] the experimental evidence is quite limited. One of the best characterized systems is the nacre of the mollusk shell. On the basis of X-ray and electron diffraction studies, a strong correlation was observed between the spatial arrangement of carboxylate groups on the antiparallel β-pleated sheet and Ca^{2+} ion distributions in the (001) surface of aragonite.[94] Our speculations regarding the temptation formation from the α-helical conformation of the peptide could be consistent with such a model. As noted above, though, few other systems have been identified with unequivocal matching of protein template sites with biomineral crystal parameters.

Once the crystal has been nucleated, BSP may also influence the crystal growth stage of biomineralization. In our simulation, we show that it is possible for the peptide in helical conformation to generate a Ca^{2+} equilateral triangle template, so it might not be unreasonable to hypothesize that through such a potential crystal pattern matching, BSP may bind an existing hydroxyapatite crystal in helical conformation, thus, controlling crystal growth of the (001) crystal face. In fact, the binding of peptides in helical conformation with hydroxyapatite has been observed for other protein systems.[95−97] The N-terminus of statherin contains phosphorylated serine residues and contiguous glutamic acid residues (DSpSpEEK) similar to the binding motifs of BSP.[98,99] Using solid-state NMR, Long et al. found that the N-terminus of statherin is α-helical in character when bound to the hydroxyapatite surface.[95] A high-resolution (2.0 Å) X-ray crystal structure of porcine osteocalcin showed that five γ-carboxylated glutamic acids (Gla) coordinate five Ca^{2+} ions in a spatial orientation that is complementary to Ca^{2+} in a hydroxyapatite crystal lattice of (100) surface.[100] The five Gla residues belong to two neighboring helixes. Interestingly, we identify for the first time that the highly conserved Ca^{2+}-binding residues of Gla 17, 21, and 24 on α-helix 1 in osteocalcin also satisfies the residue sequence pattern discussed above, i.e., n, $n + 4$, $n + 7$, although the Ca^{2+} ions are identified in a rather linear geometry and match with different surfaces of hydroxyapatite. Clearly, it is of great interest to explore interactions of BSP with hydroxyapatite crystal faces at the atomic level using MD simulations, which are in progress in our group.

5. Conclusions

BSP has been suggested to be a potential hydroxyapatite nucleator in the bone matrix. The highly conserved contiguous Glu sequences have been demonstrated to be the nucleating domains. However, the structures of the nucleating domains are not experimentally resolved to date, which hinders further study of the detailed nucleating mechanism. In the present work, we performed MD simulation to study the conformational effect of a BSP nucleating motif on the distributions of Ca^{2+} and Pi ions in solution, and specifically, we explored whether a nucleation template for orientated hydroxyapatite could be formed in different peptide conformations. The corresponding inorganic solutions were also studied as a reference. For most of our simulations, independent of peptide conformations, no apparent nucleation template for the hydroxyapatite crystal lattice is observed. Thus, BSP is more likely to promote the nucleation of the amorphous calcium phosphate. In some of the simulations of the α-helical conformation, the possibility of promoting templated nucleation of the hydroxyapatite was seen. However, considering that template formation was not general (not observed for all starting configurations) and robust (not observed for all long period simulations), the templating effect with the helical conformation is not likely to be the dominant mechanism. It would be particularly interesting and important if the nucleation process of the hydroxyapatite promoted by the model peptide could be studied experimentally. Careful characterization of the first-formed phase of calcium phosphate with presence

(84) Lowenstam, H. A.; Weiner, S. *Science* **1985**, *227*, 51.
(85) Mahamid, J.; Sharir, A.; Addadi, L.; Weiner, S. *Proc. Natl. Acad. Sci. U.S.A.* **2008**, *105*, 12748.
(86) Yang, X. D.; Wang, L. J.; Qin, Y. L.; Sun, Z.; Henneman, Z. J.; Moradian-Oldak, J.; Nancollas, G. H. *J. Phys. Chem. B* **2010**, *114*, 2293.
(87) Gotliv, B. A.; Addadi, L.; Weiner, S. *ChemBioChem* **2003**, *4*, 522.
(88) Weiss, I. M.; Tuross, N.; Addadi, L.; Weiner, S. *J. Exp. Zool.* **2002**, *293*, 478.
(89) Politi, Y.; Metzler, R. A.; Abrecht, M.; Gilbert, B.; Wilt, F. H.; Sagi, I.; Addadi, L.; Weiner, S.; Gilbert, P. *Proc. Natl. Acad. Sci. U.S.A.* **2008**, *105*, 17362.
(90) Politi, Y.; Levi-Kalisman, Y.; Raz, S.; Wilt, F.; Addadi, L.; Weiner, S.; Sagi, I. *Adv. Funct. Mater.* **2006**, *16*, 1289.
(91) Politi, Y.; Arad, T.; Klein, E.; Weiner, S.; Addadi, L. *Science* **2004**, *306*, 1161.
(92) Killian, C. E.; Metzler, R. A.; Gong, Y. U. T.; Olson, I. C.; Aizenberg, J.; Politi, Y.; Wilt, F. H.; Scholl, A.; Young, A.; Doran, A.; Kunz, M.; Tamura, N.; Coppersmith, S. N.; Gilbert, P. U. P. A. *J. Am. Chem. Soc.* **2009**, *131*, 18404.
(93) Addadi, L.; Berman, A.; Oldak, J. M.; Weiner, S. *Connect. Tissue Res.* **1989**, *21*, 457.
(94) Weiner, S.; Talmon, Y.; Traub, W. *Int. J. Biol. Macromol.* **1983**, *5*, 325.
(95) Long, J. R.; Shaw, W. J.; Stayton, P. S.; Drobny, G. P. *Biochemistry* **2001**, *40*, 15451.
(96) Makrodimitris, K.; Masica, D. L.; Kim, E. T.; Gray, J. J. *J. Am. Chem. Soc.* **2007**, *129*, 13713.
(97) Masica, D. L.; Gray, J. J. *Biophys. J.* **2009**, *96*, 3082.
(98) Long, J. R.; Dindot, J. L.; Zebroski, H.; Kiihne, S.; Clark, R. H.; Campbell, A. A.; Stayton, P. S.; Drobny, G. P. *Proc. Natl. Acad. Sci. U.S.A.* **1998**, *95*, 12083.
(99) Schlesinger, D. H.; Hay, D. I. *J. Biol. Chem.* **1977**, *252*, 1689.
(100) Hoang, Q. Q.; Sicheri, F.; Howard, A. J.; Yang, D. S. C. *Nature* **2003**, *425*, 977.

of designed peptides is highly encouraged to carry out in wet laboratories.

Acknowledgment. This research was funded by a National Scientific Foundation CAREER Award (EAR 0346689), American Chemical Society Petroleum Research Fund (41777-AC2), and NASA Astrobiology Institute grant to N.S., and by partial postdoctoral salary support to Y.Y. from the Department of Geoscience Weeks Endowment. Y.Y. thanks Dr. Liang Ma for helpful discussions on some technical details. Computational resources from the National Center for Supercomputing Applications (NCSA) at the University of Illinois and the Condor High Throughput Computing (CHTC) at the University of Wisconsin are greatly appreciated. N.S. is grateful to Prof. Mel Glimcher and Drs. Yaotang Wu, Jeery Ackerman and Erdjan Salih for introducing her to the concepts of phosphoproteins and bone mineralization and for useful discussions on the topic.

Supporting Information Available: Test giving the method and figures showing the results for the distance matrices calculation, representative structures for Ca−P clusters from the inorganic solution, solvent accessible surface area (SASA) for peptides, CHARMM force field parameters for HPO_4^{-}, $H_2PO_4^{2-}$, and Ca^{2+}, structure analysis for the Ca^{2+} equilateral triangle for the additional simulations for the pα12_Ca_Pi_NaCl system are provided in the supporting materials, and tables of partial charges and van der waals parameters. This material is available free of charge via the Internet at http://pubs.acs.org.

Supporting Materials for

How does bone sialoprotein promote the nucleation of hydroxyapatite? A molecular dynamics study using model peptides of different conformations

Yang Yang[1], Qiang Cui[2], Nita Sahai[1, 3, 4 *]

[1]*Department of Geoscience*
University of Wisconsin, Madison
1215 West Dayton Street, Madison, WI 53706

[2]*Department of Chemistry and Theoretical Chemistry Institute*
University of Wisconsin, Madison
1101 University Ave, Madison, WI 53706

[3]*Materials Science Program*
University of Wisconsin, Madison
1509 University Ave, Madison, WI 53706

[4]*Environmental Chemistry and Technology Program*
University of Wisconsin, Madison
680 North Park Street, Madison, WI 53706

*****Corresponding author: Nita Sahai, sahai@geology.wisc.edu, 608-262-4972 (tel), 608-262-0693 (fax)

Method to calculate distance matrix

To analyze formation of clusters in solutions containing only inorganic ions, distance matrices are computed for Ca^{2+}-Ca^{2+} and P-P pairs, where P is the phosphorus atom of the Pi. The detailed calculation scheme is: (1) divide the whole production trajectory into 4 segments to address the dynamic features of the cluster, with 1 ns for each segment; (2) within each segment, for every frame, calculate the Ca^{2+}-Ca^{2+} or P-P distance for every Ca^{2+}-Ca^{2+} or Pi-Pi pair. For example, for the system of Ca_H_2PO_4_NaCl, there are 10 Pi (thus 45 different P-P distances); to generate a complete square matrix, 100 pairwise distances are computed including double counting; (3) for each segment, in total, there are 1000 frames. Calculate the average value for the Ca^{2+}-Ca^{2+} and P-P distances over the 1000 frames. If the averaged Ca^{2+}-Ca^{2+} or P-P distance is shorter than 8.0 Å, the distance value is kept, otherwise, it is zeroed out; (4) based on the average distance, generate a matrix, where the row and column are the Ca^{2+} or Pi indices (Ca^{2+} 1, Ca^{2+} 2, … or Pi 1, Pi 2, ...), and the value in the matrix is the average distance between the two indexed ions; (5) convert the numerical matrix to a 3-dimensional contour plot; (6) compute the matrices for every segment mentioned in step (1).

Partial charges and van der Waals parameters for HPO_4^-, $H_2PO_4^{2-}$, and Ca^{2+} are shown.

Table 1. Partial charges for ions used in simulations.

Molecule	Atom	Charge (e)
Ca^{2+}	Ca	2.00
$H_2PO_4^-$	P	1.04
	O	-0.72
	O(H)[a]	-0.63
	H	0.33
HPO_4^{2-}	P	1.10
	O	-0.90
	O(H)	-0.73
	H	0.33

Note: a) O(H) is the protonated oxygen.

Table 2. van der Waals parameters for ions used in simulations.

Atom	ε (kcal/mol)	$R_{min}/2$ (Å)
Ca	-0.1200	1.3670
P	-0.5850	2.1500
O	-0.1200	1.7000
O(H)[a]	-0.1521	1.7700
H	-0.0460	0.2245

Note: a) O(H) is the protonated oxygen.

Figure Caption

Figure S1. Side lengths (a, b, c) and circumference (d, e, f) for the Ca^{2+} equilateral triangle formed with Ser2, Glu6, and Glu9 from the three additional simulations for the pα12_Ca_Pi_NaCl system. The green line indicates the corresponding value for the (001) surface of the hydroxyapatite crystal.

Figure S2. Inorganic phosphate distance matrices for the Ca_H_2PO_4_NaCl system. See method section for calculation details. Distance are in angstrom.

Figure S3. Ca^{2+} distance matrices for the Ca_H_2PO_4_NaCl system. See method section for calculation details. Distance are in angstrom.

Figure S4. Inorganic phosphate distance matrices for the Ca_HPO_4_NaCl system. See method section for calculation details. Distance are in angstrom.

Figure S5. Ca^{2+} distance matrices for the Ca_HPO_4_NaCl system. See method section for calculation details. Distance are in angstrom.

Figure S6. Representative cluster structures from the Ca_HPO_4_NaCl system.

Figure S7. Solvent accessible surface area (SASA) for both peptide charge states (a) for the p10 system; (b) for the p12 system.

Figure S1

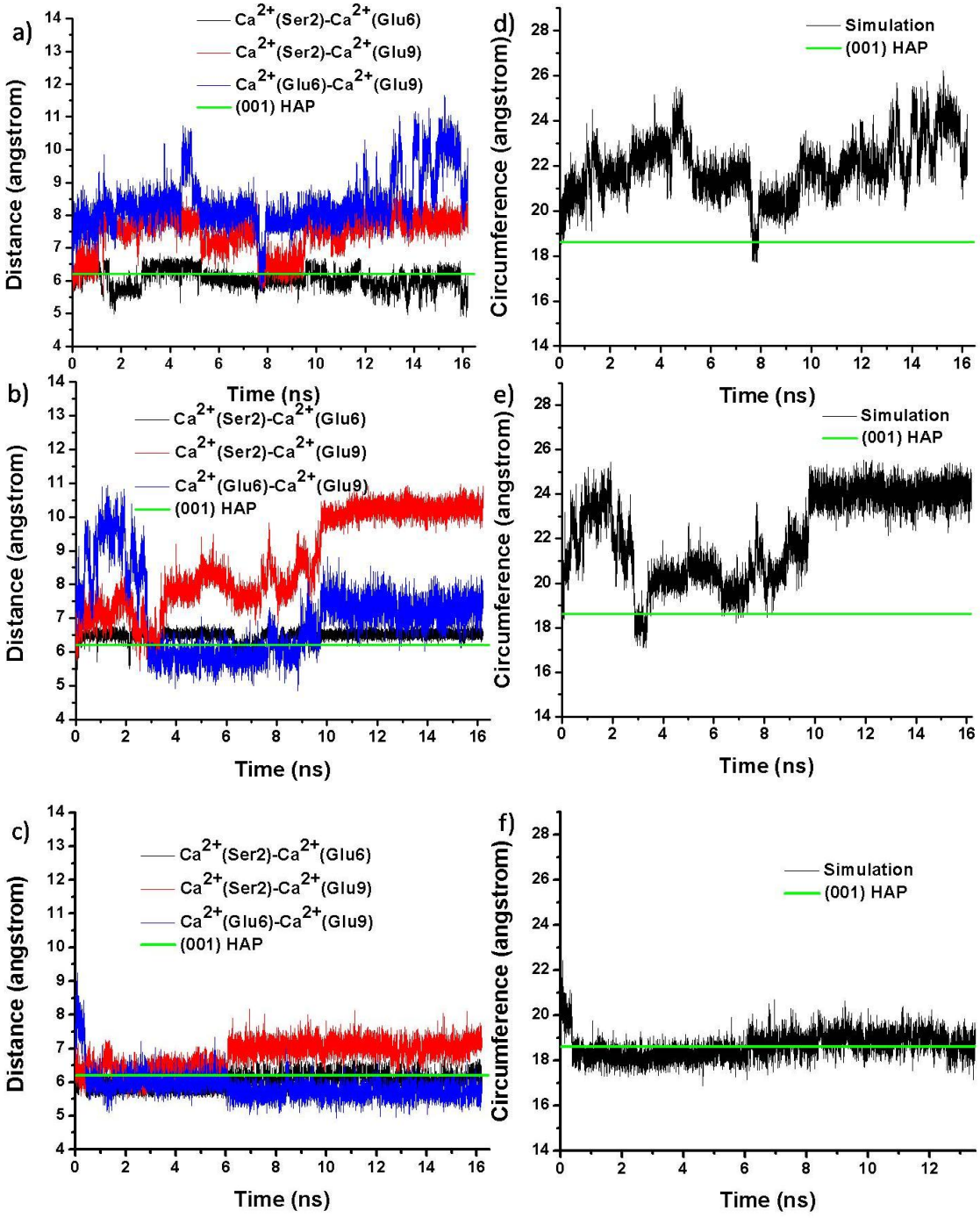
a)
b)
c)
d)
e)
f)
Distance (angstrom)
Circumference (angstrom)
Time (ns)
Ca2+(Ser2)-Ca2+(Glu6)
Ca2+(Ser2)-Ca2+(Glu9)
Ca2+(Glu6)-Ca2+(Glu9)
(001) HAP
Simulation

Figure S2

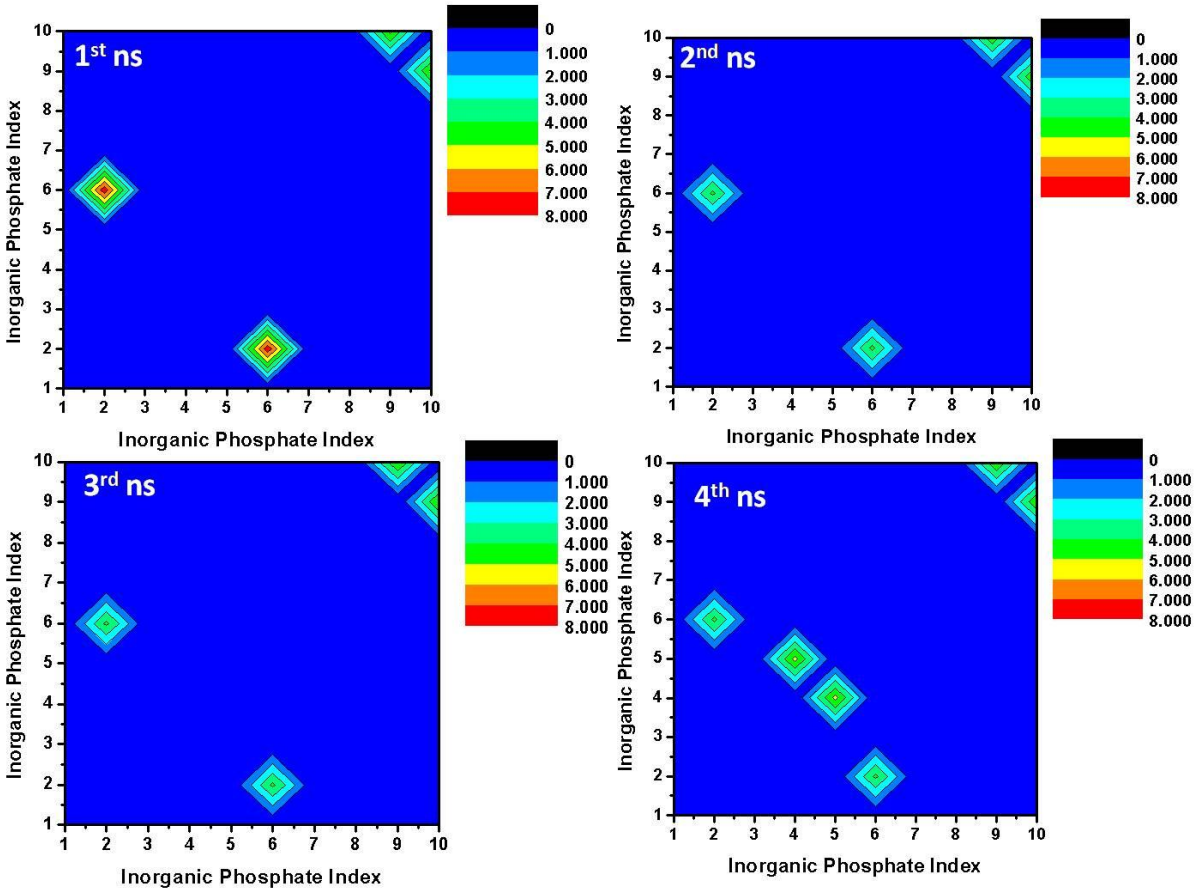
1st ns
2nd ns
3rd ns
4th ns
Inorganic Phosphate Index
Inorganic Phosphate Index
0
1.000
2.000
3.000
4.000
5.000
6.000
7.000
8.000

Figure S3

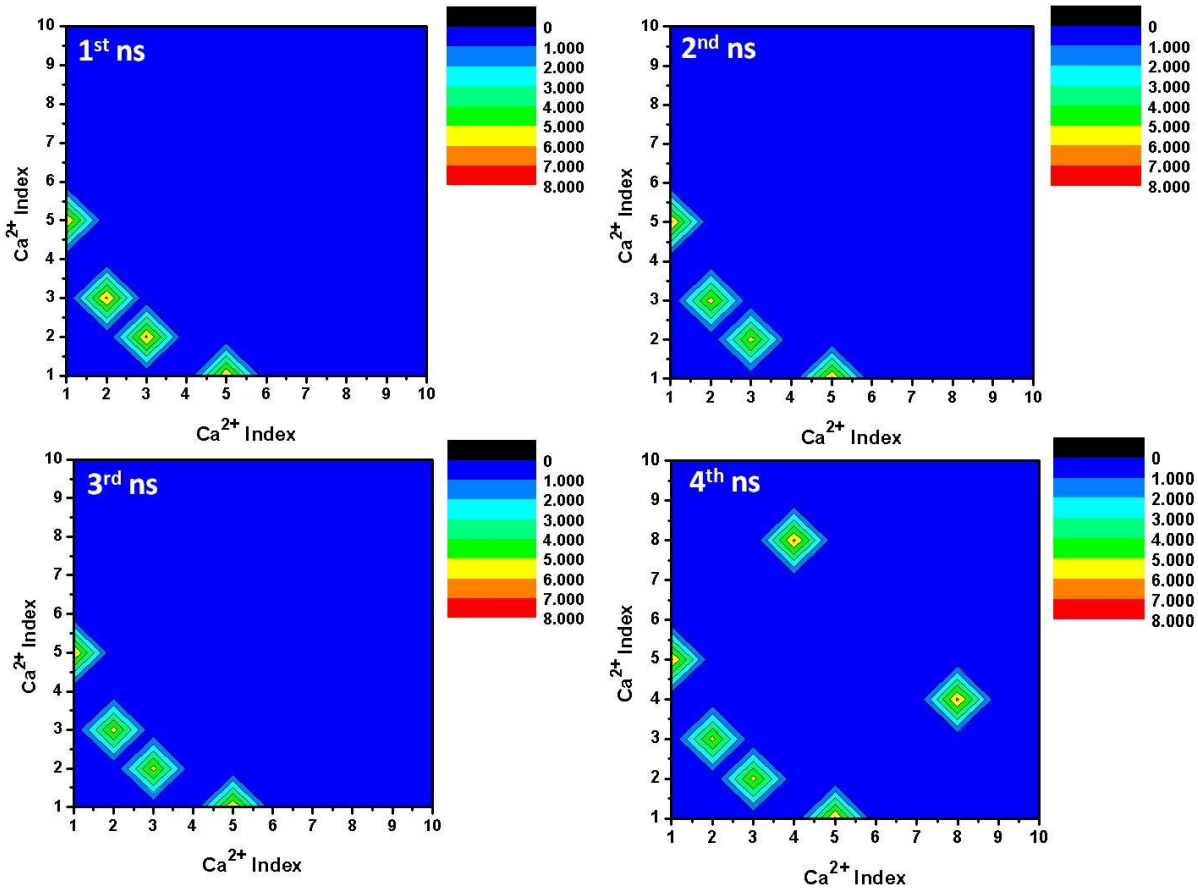
1st ns
2nd ns
3rd ns
4th ns
Ca2+ Index
Ca2+ Index
0
1.000
2.000
3.000
4.000
5.000
6.000
7.000
8.000

Figure S4

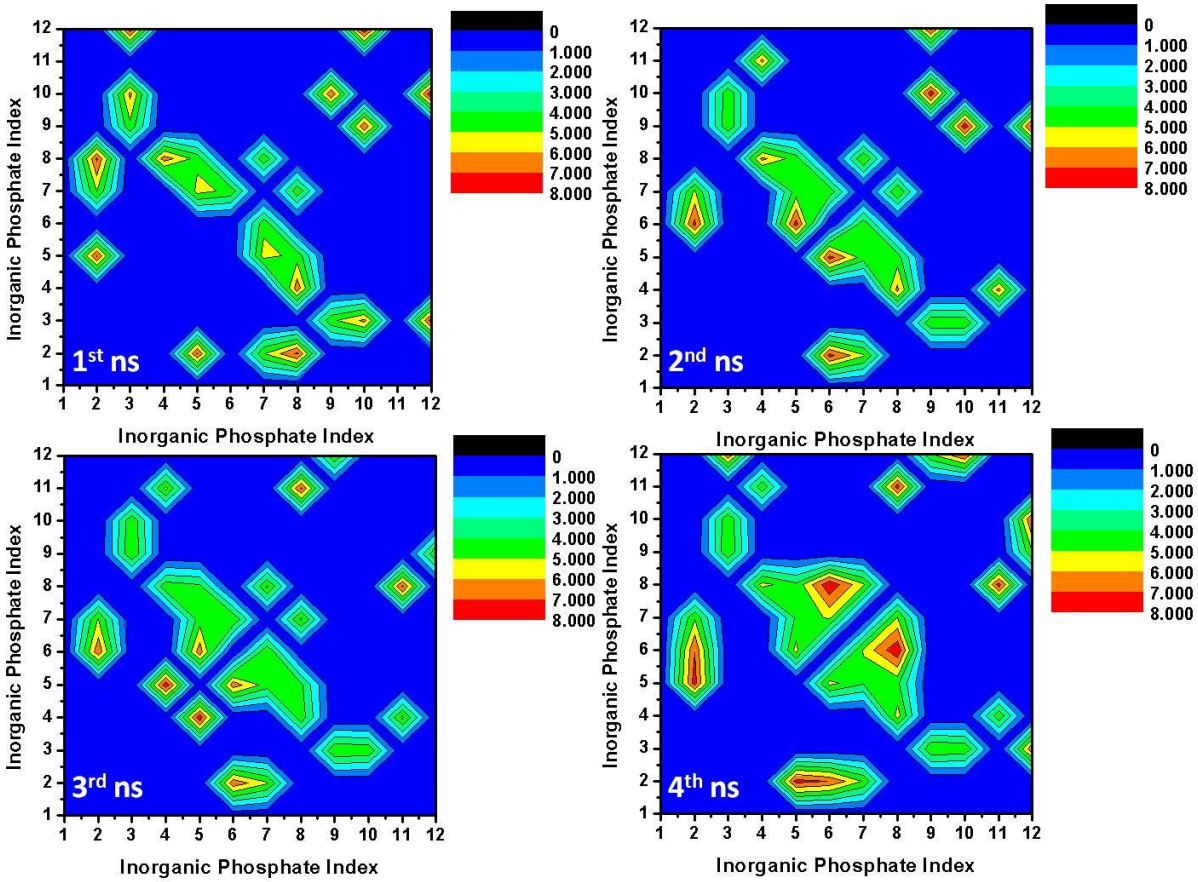
1st ns
2nd ns
3rd ns
4th ns
Inorganic Phosphate Index
Inorganic Phosphate Index
0
1.000
2.000
3.000
4.000
5.000
6.000
7.000
8.000

Figure S5

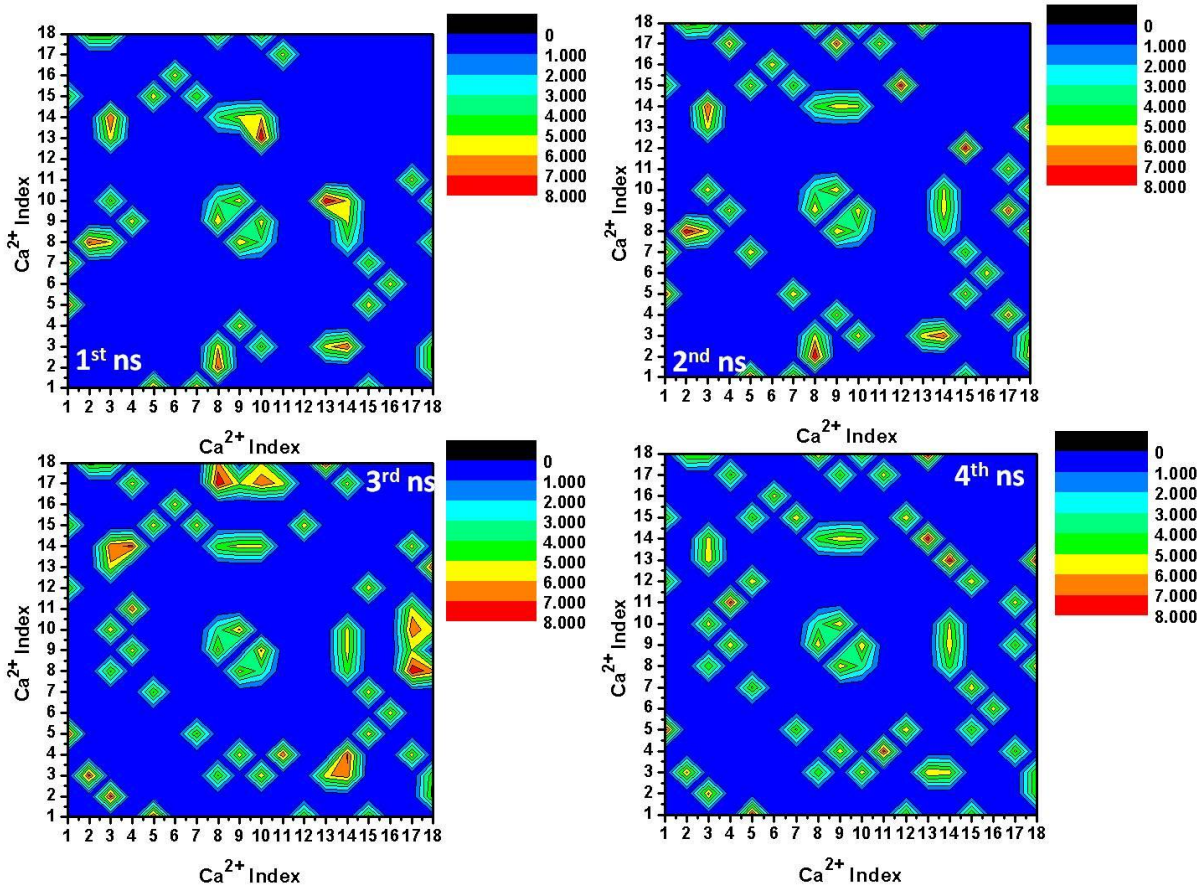
1st ns
2nd ns
3rd ns
4th ns
Ca2+ Index
Ca2+ Index
0
1.000
2.000
3.000
4.000
5.000
6.000
7.000
8.000

Figure S6

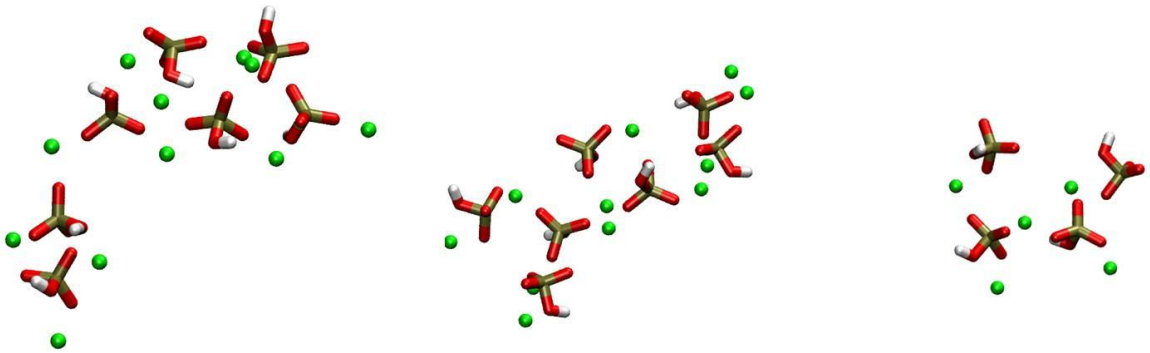

Figure S7

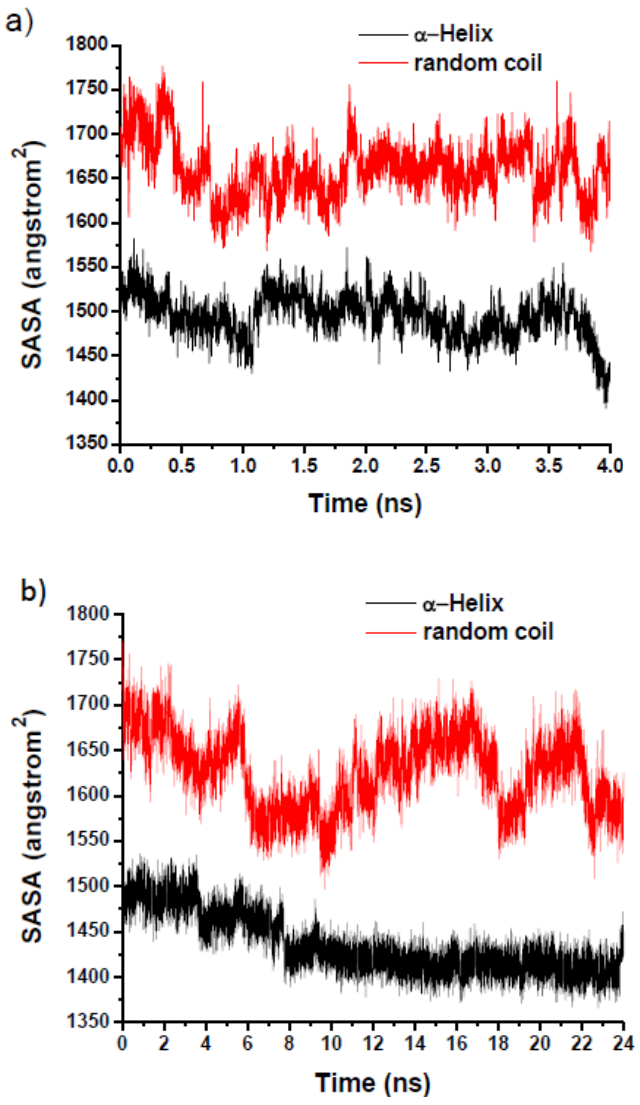
a)
α–Helix
random coil
SASA (angstrom^2)
1800
1750
1700
1650
1600
1550
1500
1450
1400
1350
0.0
0.5
1.0
1.5
2.0
2.5
3.0
3.5
4.0
Time (ns)
b)
α–Helix
random coil
SASA (angstrom^2)
1800
1750
1700
1650
1600
1550
1500
1450
1400
1350
0
2
4
6
8
10
12
14
16
18
20
22
24
Time (ns)